Monthly Notices of the ROYAL ASTRONOMICAL SOCIETY

MNRAS **509,** 4694–4712 (2022) https://doi.org/10.1093/mnras/stab3240
Advance Access publication 2021 November 10

Modelling multiwavelength emission of Ultra-luminous X-ray Sources accreting above the Eddington limit

E. Ambrosi,[1]★ L. Zampieri [2], F. Pintore [1,3] and A. Wolter [4]

[1]*INAF - IASF Palermo, Via U. La Malfa 153, I-90146 Palermo, Italy*
[2]*INAF-Osservatorio Astronomico di Padova, vicolo dell'Osservatorio,5, I-35122 Padova, Italy*
[3]*INAF - IASF Milano, via E. Bassini 15, I-20133 Milano, Italy*
[4]*INAF, Osservatorio Astronomico di Brera, via Brera 28, I-20121 Milano, Italy*

Accepted 2021 November 4. Received 2021 November 4; in original form 2021 May 12

ABSTRACT

We model the multiwavelength properties of binaries accreting at super-critical rates with the aim to better understand the observational properties of Ultra-luminous X-ray Sources (ULXs). We calculate an extended grid of binary systems which evolve through Roche Lobe Overflow and undergo case A mass transfer from massive donors (up to 25 $M_\odot$) on to massive black holes (BHs) (up to 100 $M_\odot$). Angular momentum loss with the ejection of mass through an outflow is incorporated. We apply our super-Eddington accretion model to these systems, computing their evolutionary tracks on the colour–magnitude diagram (CMD) for the Johnson and *Hubble Space Telescope* photometric systems. We found that the tracks occupy specific positions on the CMD depending on the evolutionary stage of the donor and of the binary. Moreover, their shapes are similar, regardless the BH mass. More massive BHs lead to more luminous tracks. We additionally compute their optical-through-X-ray spectral energy distribution considering the effects of a Comptonizing corona that surrounds the innermost regions of the disc. We apply our model to four ULXs: NGC 4559 X-7, NGC 5204 X-1, Holmberg II X-1, and NGC 5907 ULX-2. We found that accretion on to BHs with mass in the range of 35–55 $M_\odot$ is consistent with to the observational properties of these sources. We finally explore and discuss the possibility to extend our model also to ULXs powered by accreting pulsars (PULXs).

Key words: accretion, accretion discs – X-rays: binaries – X-rays: individual: NGC 4559 X-7, NGC 5204 X-1, Holmberg II X-1, NGC 5907 ULX-2.

1 INTRODUCTION

Ultra-luminous X-ray sources are point-like, off-nuclear X-ray sources whose bolometric luminosity exceeds the Eddington limit for a 10 $M_\odot$ BH ($L_{\rm Edd} \sim 2 \times 10^{39}$ erg s^{-1}; Fabbiano 1989, see Kaaret, Feng & Roberts 2017 for a recent review).

They have been discovered in nearby galaxies and are associated with different environments: star-forming regions or young stellar environments in spiral galaxies, or dwarf irregular galaxies (e.g. Ramsey et al. 2006, Pakull, Grisé & Motch 2006, Liu et al. 2007, Mineo, Gilfanov & Sunyaev 2012). In few cases, they are associated with older stellar populations in elliptical galaxies (Feng & Kaaret 2008; Roberts, Levan & Goad 2008). A large number of ULXs has been found also in the young and star-forming rings of ring galaxies (Wolter, Fruscione & Mapelli 2018). Many of them are located in or close to young O-B associations (see e.g. the population studies performed by Soria et al. 2005; Grisé et al. 2008; Goad et al. 2002), often embedded in low-metallicity environments and/or high star-forming regions (Mapelli et al. 2011; Wolter et al. 2015).

Their observational properties, as the X-ray luminosity, the variability and the spectral changes indicate that the majority ULXs are likely compact objects accreting via a disc (Makishima et al. 2000; Feng & Soria 2011).

Early on, their high X-ray luminosities suggested that the mass of the compact object was higher than the average masses of the BHs observed in our Galaxy if standard accretion occurs. It was proposed (Colbert & Mushotzky 1999) that they could host Intermediate Mass Black Holes (IMBHs) with masses of $\sim 10^3 - 10^5$ $M_\odot$.

However, further investigations revealed also that their X-ray spectral properties are unusual if compared to those observed in Galactic X-ray Binaries (XRBs; Mizuno, Kubota & Makishima 2001) opening the possibility to explain ULXs in terms of alternative accretion disc scenarios, without invoking IMBHs. It was proposed that super-Eddington accretion discs, as the slim discs models, around stellar-mass or slightly more massive BHs, could reproduce the spectra of ULXs (Ebisawa et al. 2003).

A significant effort was devoted in recent years to understand the nature of ULXs. With the advent of more sensitive X-ray telescopes (*Chandra, XMM–Newton, NuSTAR*), the spectral properties of ULXs could be analysed in greater detail. Roberts (2007), Gladstone, Roberts & Done (2009), and Sutton, Roberts & Middleton (2013b) identified the so-called *Ultra luminous state*, which is characterized by the presence of some important features in ULXs spectra. This led to the conclusion that ULXs should be stellar-mass or massive (up to 100 $M_\odot$) BHs accreting with marginally or highly super-Eddington rates from massive donors. In fact, Belczynski et al. (2008), Mapelli,

★ E-mail: elena.ambrosi@inaf.it

Colpi & Zampieri (2009), and Zampieri & Roberts (2009) explored the massive BH scenario, finding that low-metallicity environments could lead to the formation of BHs in the range of 30–80 $M_\odot$ and that marginal super-Eddington accretion on to these BHs could explain the observed properties of ULXs.

Understanding the nature of ULXs became more and more challenging after the discovery of the first pulsating ULX (Bachetti et al. 2014), which unequivocally showed that ULXs can also be accreting neutron stars. This discovery has been confirmed by the identification of other five pulsar ULXs (Israel et al. 2017a, b; Carpano et al. 2018; Rodríguez Castillo et al. 2019; Sathyaprakash et al. 2019) whose emission properties can only been explained in terms of super-Eddington accretion (Mushtukov et al. 2017).

ULXs appear to be the sources where super-Eddington accretion reveals itself in a variety of phenomenological modes. A strong evidence of such an extreme regime is also the presence of outflows, inferred from the detection of radio, optical and X-ray giant nebulae (Pakull & Mirioni 2002; Miller, Fabian & Miller 2005; Belfiore et al. 2020), broad optical emission lines (Fabrika et al. 2015) and blue-shifted X-ray absorption lines (e.g. Pinto, Middleton & Fabian 2016; Pinto et al. 2017).

The main goal of this work is to investigate the nature of ULXs using their multiwavelength emission properties along with binary evolution in the context of super-Eddington accretion.

In Section 2, we present the evolutionary tracks of simulated ULX binaries with BHs and their emission properties. The third section is devoted to the comparison of our model with some nearby and well-studied ULXs. Finally, in the last section we explore the possibility to extend our model to the case of PULXs.

2 EVOLUTIONARY TRACKS OF ULXS AND THEIR OPTICAL APPEARENCE

In this section, we compute the evolutionary tracks of binary ULXs and their optical emission throughout it. Following previous work, Belczynski et al. (2008), Patruno & Zampieri (2008, hereafter PZ1), Mapelli et al. (2009), Zampieri & Roberts (2009), and Patruno & Zampieri (2010, hereafter PZ2), here we assume that these systems are high-mass X-ray binaries, and that the compact object is a black hole which is accreting matter from a massive donor via Roche lobe overflow. We further asssume that the mass transfer process starts when the donor is on the main sequence (MS; case A mass transfer, see Eggleton 2006).

2.1 MESA evolutionary tracks

We used the stellar evolution code MESA (Modules for Experiments in Stellar Astrophysics, release 10108, Paxton et al. 2011, 2013, 2015), to run a set of representative ULX binaries accreting via Roche Lobe Overflow.

We considered donors with masses in the range 530$M_\odot$ and BH masses in the range of 10–100$M_\odot$. In this work, the donor metallicity is fixed at the solar value ($Y = 0.28$, $Z = 0.02$). However, we tested the validity of this approximation and evolved some binaries with sub-solar metallicity. The resulting tracks (see Appendix A) show that this is a valid approximation for the scope of this work. We also underline that Klencki et al. (2020) studied the effects of metallicity on binary evolution, and found that it plays an important role only for those systems which start the accretion phase when the donor is an evolved star (case B mass transfer). As we focus our analysis on systems that start mass transfer on the MS (case A mass transfer), in the following we consider the assumption of solar metallicity acceptable.

We took into account the effects of the wind mass-loss, which affects significantly the evolution of massive donors. Among the wind schemes that can be implemented, we chose the method that in MESA is called 'Dutch wind scheme', which differentiates the wind mass-loss prescription for the stars in the MS from that after the MS, following the work by Glebbeek et al. (2009). For the MS we used the default input relation (Vink, de Koter & Lamers 2001, 2000). For the evolved stars we adopted the de Jager relation (de Jager, Nieuwenhuijzen & van der Hucht 1988) that, as observed by Renzo et al. (2017), is useful when the main objective is to study mass loss along the evolution on the HR diagram. We also note that in the specific systems we made evolving, i.e. during RLOF, mass loss via accretion is orders of magnitude higher than that expelled through stellar wind (see also Smith 2014 for a comprehensive review), so that we do not expect that a different wind prescription can considerably alter our results.

First, we run the *star* module for each donor mass. Then, we set the start of the RLOF phase during MS, when the central Hydrogen abundance (h1) is $\simeq$0.5 (case A mass transfer). We denote the radius of the donor at this stage with $R = R_{d,\,h1}$. The evolution is stopped at the onset of helium burning in the core.

We set the initial period for the binaries combining Kepler's law:

$$P \approx 2\pi G^{-1/2} a_1^{3/2} (M_d + M_a)^{-1/2} \tag{1}$$

with the Eggleton approximation. Under the hypothesis that $R_{d,\,h1} = R_L$ (Eggleton 1983):

$$a_1 \approx R_{d,h1} \frac{0.6q^{2/3} + \ln(1 + q^{1/3})}{0.49q^{2/3}}, \tag{2}$$

where R_L is the Roche Lobe Radius of the donor, a_1 is the initial orbital separation, M_d and M_a are the donor and accretor mass, and $q = M_d/M_a$. The initial orbital periods turn out to be in the range of 1–2 d. The RLOF is calculated with the MESA implicit scheme 'Roche Lobe'. We set the minimum mass transfer rate at $\dot{M}_{min} = 1.0 \times 10^{-12} M_\odot/yr$.

The time-step is chosen in such a way to have an adequate time resolution without excessively increasing the computational time (typically about $\sim$4–5 h). As the binary evolution proceeds faster after the Terminal Age Main Sequence (TAMS), the time resolution for the evolution of the donor during the post-MS stages is tighter than that adopted during the MS.[1] We also set to zero the initial spin of the BH, which increases as accretion proceeds.

2.1.1 *Orbital angular momentum through the outflow*

According to the model with an accretion disc plus an outflow adopted in Ambrosi & Zampieri (2018), hereafter AZ, the evolution proceeds via non-conservative mass transfer and the accretion flow is not Eddington-limited. When the mass transfer rate becomes super-critical, the mass ejected with the outflow effectively removes also orbital angular momentum. The total outflow rate depends on the fraction of radiative energy spent in launching the wind, ϵ_w, and is given by (equation 24 of Poutanen et al. 2007):

$$\dot{M}_w \approx a_w \dot{M}, \tag{3}$$

[1] setting '*varcontrol_ms*' = 1d-4 and '*varcontrol_postms*' = '*varcontrol_casea*' = '*varcontrol_caseb*' = 1d-5

where $\dot{M}$ is the mass transfer rate and, following Poutanen et al. 2007, $a_w = \epsilon_w(0.83 - 0.25\epsilon_w)$. We assume that half of the radiative energy accelerates the outflow ($\epsilon_w = 0.5$) and then $a_w = 0.3525$.

As the outflow is launched from the inner disc where the radiation pressure is higher, we assume that matter leaves the system from the vicinity of the BH. The resulting orbital angular momentum loss is implemented in MESA following Soberman, Phinney & van den Heuvel (1997):

$$\frac{\dot{J}_{ml}}{J_{orb}} = \frac{\alpha + \beta q^2 + \delta\gamma(1+q)^2}{1+q}\frac{\dot{M}_d}{M_d}, \quad (4)$$

where α is the fraction of the mass lost from the donor, β that expelled from the zones near the accretor, and δ that expelled from a circumbinary planar toroid with radius $r_t = \gamma^2 a$ (we refer to van den Heuvel 1994 and Paxton et al. 2015 for details). According to equations (4) and (3), we then set $\beta = a_w = 0.3525$, $\alpha = \delta = \gamma = 0$.

2.1.2 *Evolutionary tracks*

The evolution of the mass transfer rate for the systems considered here is shown in Fig. 1. The tracks are grouped together according to the initial BH mass and colour-coded according to the initial donor mass. We describe the evolution of the tracks taking as reference the systems accreting on to a 10$M_\odot$ BH. They span a wide range in the mass ratio q, which is an important parameter driving the evolution of accreting binaries (see Eggleton 2011). We distinguish three different evolutionary paths.

For very massive donors of 25 and 30 $M_\odot$ ($q = 2.5$ and $q = 3$, respectively), the accretion phase starts abruptly with an instability, reaching high rates (up to $10^{-1} - 1 M_\odot$ yr^{-1}, see the top left-hand panel of Fig. 1). The time-scale for mass transfer ($\tau_{\dot{m}} = M/\dot{M}$) is faster than the thermal time-scale, as shown in the top left-hand panel of Fig. 2: τ_{KH}[2] is up to six orders of magnitude larger than $\tau_{\dot{m}}$. Moreover, as the donor loses mass, it is driven rapidly towards instability, being the mass transfer rate higher than the maximum value permitted by the condition of hydrostatic equilibrium (see Pols 2011 and the second and third left-hand panels of Fig. 2). This effect is likely to lead the system towards a common envelope (CE) phase. This particular phase of binary evolution needs a dedicated modelling with physical assumptions different from those adopted for RLOF accretion, which is the relevant mechanism considered here for persistent ULXs. For this reason, we stop the evolution of these systems at this stage, and postpone the inclusion of the CE phase in our model to a future paper.

Donors with initial mass of 15 and 20 $M_\odot$ ($q = 1.5$ and $q = 2$, respectively) go through the first, thermal unstable mass transfer episode but do not become dynamically unstable: $\tau_{\dot{m}}$ is shorter than τ_{KH} (the top left-hand panel of Fig. 2) but the ratio between the dynamical time-scale and the mass transfer time-scale decreases driving the system towards stability (the middle left-hand panel of Fig. 2). As they lose mass, and the BH grows, the mass ratio decreases, the system detaches, and the donor restores the thermal equilibrium. Thereafter, mass transfer is stable and proceeds on the nuclear time-scale. We emphasize the extreme properties of the track of the 20 $M_\odot$ donor: after having lost more than 50 per cent of its mass during the first fast episode, the system widens and detaches. The donor restart RLOF at about TAMS.

For lower donor masses with $q \leq 1$, the evolution does not go through the first unstable phase of mass transfer, but it proceeds smoothly up to the TAMS, being the mass transfer timescale longer than both the Kelvin–Helmholtz and dynamical time-scales. Accretion during the giant phase proceeds with high accretion rates, but the donors maintain both hydrostatic and thermal equilibrium.

The evolution of systems accreting on to more massive BHs proceeds in a similar way but the initial accretion episode is less extreme for the more massive donors. For the 20$M_\odot$ BH, the 25 $M_\odot$ and 30 $M_\odot$ donors can restore thermal and dynamical equilibrium, at variance with the 10 $M_\odot$ case. For the 50 $M_\odot$ BH the evolution is always stable (right panels of Fig. 2). Accretion is super-Eddington only during the giant phase.

Figs 3(a)–(f) show the evolution of a few chosen parameters of the binary systems: donor and BH mass (upper and lower left-hand panels), orbital period, and mass ratios (upper and lower right-hand panels of each figure). The 5 $M_\odot$ donor is almost totally stripped irrespectively of the BH mass (see dashed dark blue lines in the upper left-hand panels). Being its mass almost totally stripped, MESA could not find a convergent solution during the final phases and then its evolution was stopped before the onset of He burning in the nucleus. From Figs 3(a)–(f), we see that irrespectively of the BH mass, the final orbital period is shorter for systems with more massive donors. For a given BH mass, the final orbital period for 8$M_\odot$ donors can be one order of magnitude longer than that of a 30$M_\odot$ donor. Finally, we emphasize that the accretion process changes dramatically the masses of the binary components. Donors lose more than 50 per cent of their initial mass, as shown in the upper left-hand panels of Figs 3(a)–(f). BHs acquire $\sim$2 $M_\odot$ from 5 $M_\odot$ donors (dark blue lines in Figs 3a–f) and $\sim$10 $M_\odot$ from 30 $M_\odot$ donors (dark red lines in Figs 3b–f).

2.2 Optical emission of ULXs

2.2.1 *Effects of super-Eddington accretion on optical emission*

To determine the emission properties of accreting ULXs, we applied the model described in AZ to the evolutionary tracks of the systems reported in the previous section. The model computes the optical emission in the UBVRI Johnson and in the *HST* WFPC2, ACS, and WFC3 photometric systems, which can be used to make a detailed comparison with the observed optical counterparts of ULXs. The optical emission of accreting binary systems is produced by different components, each contributing with a different weight to the total optical emitted flux, depending on the accretion regime and evolutionary stage. These components are as follows:

(i) The donor star, the properties of which are different from that of an isolated star with the same initial mass (see Copperwheat et al. 2005; PZ1; PZ2; Eggleton 2011; Pols 2011 for details): during RLOF, its radius is constrained to be the Roche lobe radius and its temperature is determined by the condition of thermal equilibrium. Moreover, it can be heated up by the X-ray flux is produced by the disc.

(ii) The outer portion of the accretion disc that, for both sub-Eddington and super-Eddington accretion, is a standard Shakura & Sunyaev disc, and emits an optical flux proportional to the mass transfer rate. This region can reprocess and thermalize the X-rays from the innermost regions (see PZ1; PZ2; AZ; and references therein).

[2]The Kelvin–Helmholtz time-scale is the time scale on which a star reacts when there is disequilibrium between energy loss and energy production. It is defined as the ratio between the thermal energy content of the star E_{th} and the luminosity L: $\tau_{KH} = \frac{E_{th}}{L} \approx \frac{GM^2}{2RL} \approx 1.5 \times 10^7 \left(\frac{M}{M_\odot}\right)^2 \frac{R_\odot}{R}\frac{L_\odot}{L}$ yr

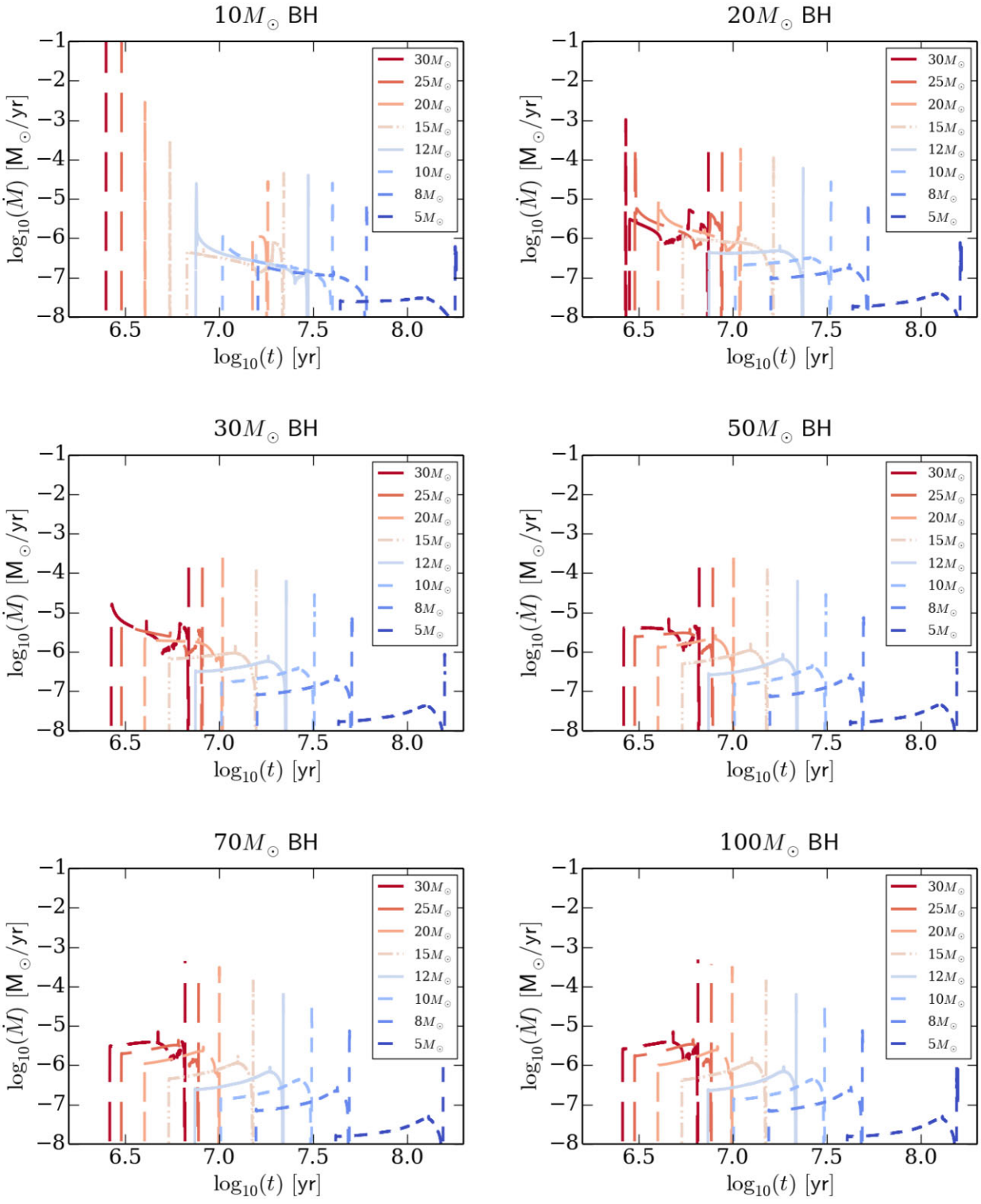

Figure 1. Evolution of the mass transfer rate for the binaries analysed in this work. The BH mass is fixed in each panel. Short dashed lines refer to donors of 5 (dark blue), 8 (blue), and 10 (light blue) $M_\odot$, solid lines to donors of 12 (azure) $M_\odot$, dashed double-dotted lines to donors of 15 (salmone) $M_\odot$, and long dashed lines to more massive donors of 20 (orange), 25 (red), and 30 (dark red) $M_\odot$.

(iii) The outflow, the radial extension of which depends on the mass transfer rate. For extremely super-Eddington accretion, the outflow produces a large amount of optical radiation, which can significantly contribute to the total luminosity and, in the more extreme regimes, be the dominant component (see AZ).

As mentioned above, a strong contribution to the optical emission comes from the reprocessing of the X-ray-UV radiation produced by the inner regions of the disc and impinging in the outer disc and the donor star. If the disc is accreting at sub-Eddington rates, the flux intercepting the outer disc and the donor star makes the latter bluer

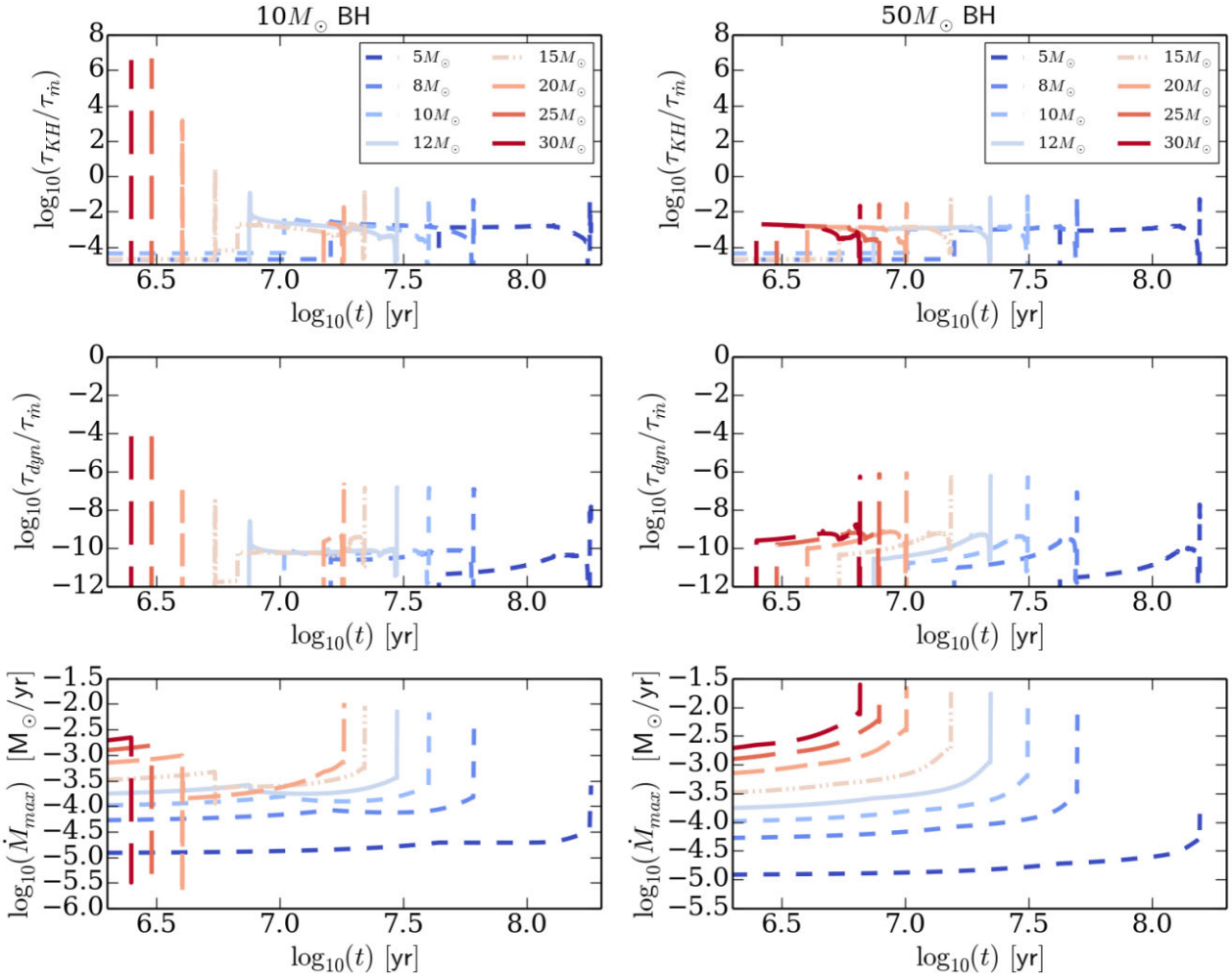

Figure 2. Evolution of the characteristic time-scales for binaries accreting on to 10 (left) and 50 (right) $M_\odot$ BHs. Upper panel: Evolution of the ratio between the Kelvin–Helmotz ($\tau_{\rm KH}$) time-scale of the donor and the characteristic time-scale for the mass transfer $\tau_{\dot{m}}$. Middle panel: Evolution of the ratio between the dynamical time-scale $\tau_{\rm dyn}$ of the donor and the mass transfer time-scale. Lower panel: Evolution of the maximum value of mass transfer achievable without perturbing the hydrostatic equilibrium of the donor.

than an isolated star with the same mass (see e.g. PZ1) and produces a bump in the red tail of the disc optical spectrum (see e.g. Sanbuichi, Yamada & Fukue 1993).

Self-irradiation for super-Eddington accretion is more complex. In AZ, we showed that the innermost regions of the disc do not irradiate the outer ones, because of the intervening outflow. The X-ray-UV irradiating flux is produced by a region located outside the outflow, the extension of which depends on the mass transfer. In addition, for extremely super-critical mass transfer rates, the region outside the photospheric radius of the outflow is too cold to produce a significant X-ray-UV flux: the disc-self-irradiation is therefore suppressed, but the intrinsic optical flux of the outer regions is very high.The size of the irradiating region in presence of an outflow is shown in Fig. 4 for all the BH masses considered. The mass transfer is normalized to Eddington, and the irradiating region to the gravitational radius. From top to bottom, the BH mass increases from 10 to 100 $M_\odot$. As already discussed in AZ, for each BH mass, the irradiating region ΔR increases with the mass transfer rate, reaches a peak, and then decreases. The more massive is the BH, the smaller is the value of $\dot{m}$ at which the irradiating region reaches its maximum ($\dot{m}_{\max,\Delta R}$). For a 100 $M_\odot$ BH, $\log_{10}(\dot{m}_{\max,\Delta R}) \sim 2.1$, while for a 10$M_\odot$ BH $\log_{10}(\dot{m}_{\max,\Delta R}) \sim 2.4$, where $\dot{m} = \dot{M}/\dot{M}_{\rm Edd}$.

2.2.2 *Evolutionary tracks on the CMD*

We computed the tracks on the colour–magnitude diagram (CMDs) of the systems described in the previous section from the onset of RLOF to the end of their evolution, which occurs while the donor ascends the giant branch. The duration of the tracks depends considerably on the donor mass: the more massive is the donor, the shorter is the evolutionary path, irrespectively of the BH mass. Systems with 30$M_\odot$ donor last about $10^{6.5}$ yr, while systems with a 5$M_\odot$ last about $10^{8.2}$ yr. The evolutionary tracks on the CMD calculated with our code (AZ) and the MESA tracks are shown in Fig. 5 ($B-V$ colour and M_V magnitude) and in Fig. 6 ($V-I$ colour and M_I magnitude). They are ordered for increasing BH mass, which is fixed in each panel. The colour code represents the magnitude of the accretion rate.

The evolutionary tracks of ULXs occupy two regions on the CMD, depending on the evolutionary stage of the donor. When the donor is on the MS and accretion is sub-critical or marginally super-critical, the tracks are blue and their M_V magnitude is limited to ~ -6. They occupy the bluer and comparatively fainter corner of the CMD, and are represented by the light-pink coloured lines in Fig. 5. We notice that they are similar in shape for different BH masses, the main

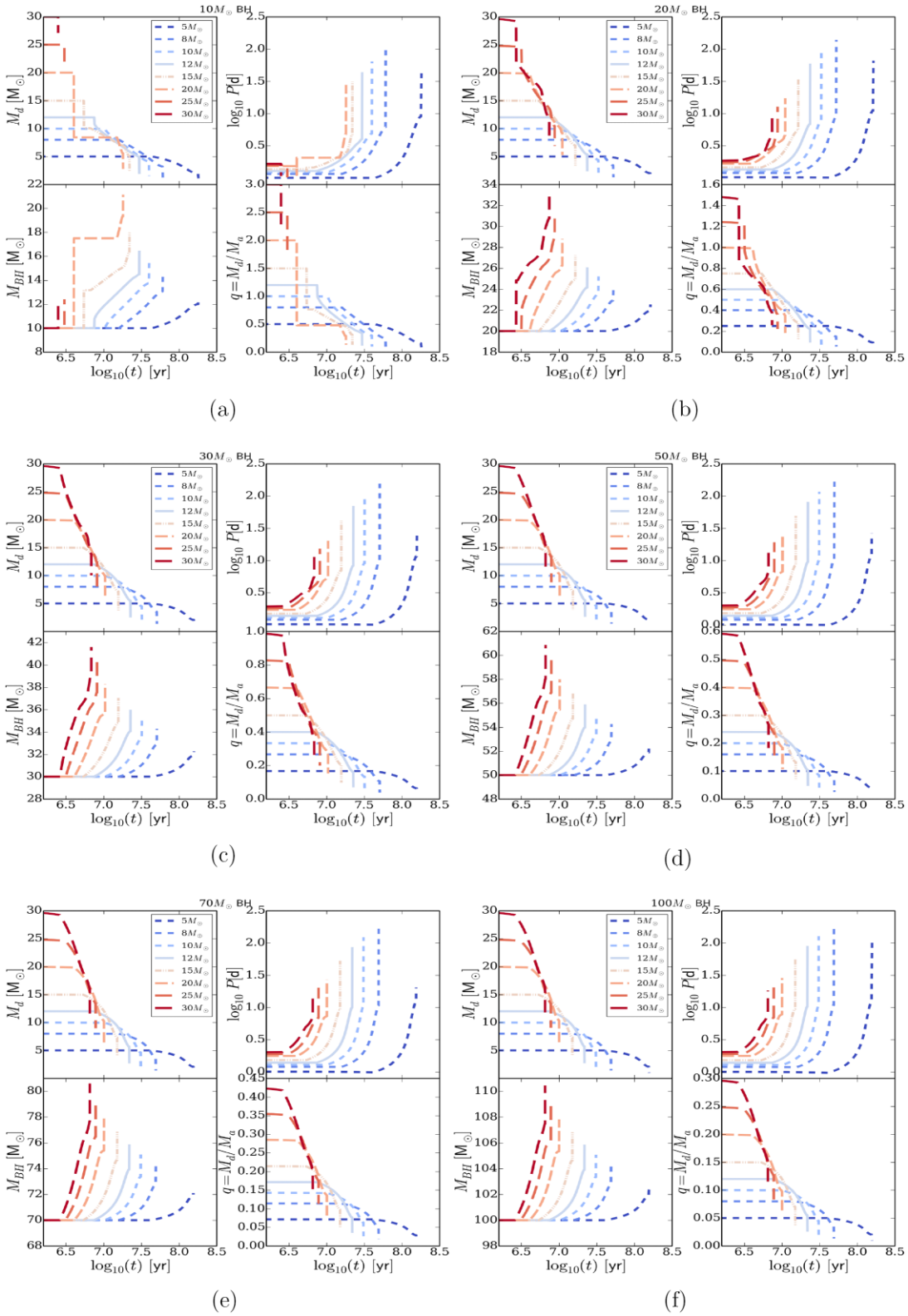

Figure 3. Evolution of the parameters for the binary systems evolved with MESA: donor mass (upper left), orbital period (upper right), BH mass (lower left), and q ratio (lower right). Systems are grouped according to the BH mass and colour-coded according to the donor mass as in Figs 1 and 2.

difference being the maximum value of M_V: more massive BHs generate more luminous tracks.

When the donor ascends towards the giant branch, the properties of the evolutionary tracks are governed by the mass transfer rate, which is now super critical, as shown in Fig. 1. Moreover, the binary separation increases rapidly producing a more extended accretion disc, which emits a huge optical flux enhanced by self-irradiation. This evolution drives the tracks towards higher V-band luminosities.

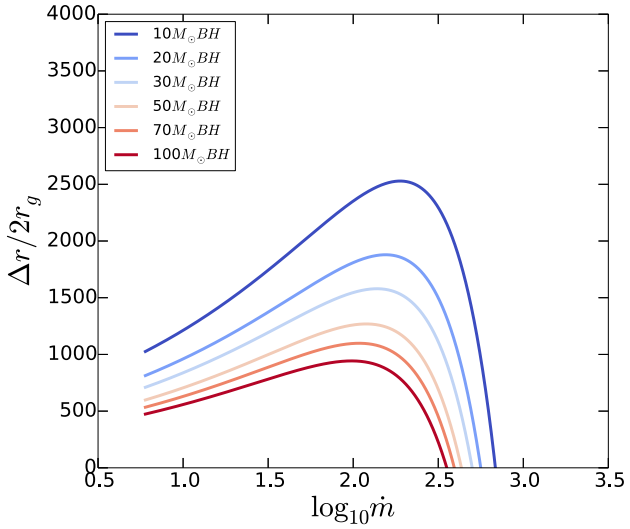

Figure 4. X-ray-UV irradiating region, $\Delta r = r_x - r_{\rm ph}$, for the binary systems evolved with MESA. r_x marks approximately the boundary of the region where the gas temperature falls within the X-rays-ultraviolet (UV) energy band, and $r_{\rm ph}$ is the outer radius of the optically thick photosphere of the outflow (details can be found in AZ). From top to bottom, the BH mass increases from 10 $M_\odot$ to 100 $M_\odot$.

The colours are initially blue because the mass transfer rate at the beginning of the giant phase is very high and the disc is hot. As the super-Eddington mass transfer continues, the systems widen and the accretion disc becomes more extended, driving the tracks towards redder colors. In addition, self-irradiation is essentially suppressed. However, after the peak, the mass transfer rate starts to decrease, irradiation starts to contribute again to the optical flux and for systems with more massive donors the evolution towards the red slows down. These super-critical evolutionary stages are reproduced with the dark pink lines in Fig. 5. We notice that the track of the 5 $M_\odot$ donor differs from the others. We will describe this case and the behaviour of the tracks for the various BH masses in Appendix B.

3 MULTIWAVELENGTH SED OF NEARBY ULXS

In AZ, we concluded that the emission of the disc plus outflow alone cannot fully reproduce the observed data, because the X-ray spectrum at the highest energies is too soft and cannot properly describe the ULXs spectra. In many ULXs observations show evidence of a spectral component that can be interpreted as an optically thick and cool corona covering the innermost regions of the disc (e.g. Gladstone et al. 2009; Pintore & Zampieri 2012; Sutton et al. 2013b). Thus, we added the contribution of a comptonizing corona, which covers the innermost regions of the disc, to the emission model of AZ.

3.1 Comptonization from an optically thick corona

We approximate the corona with a sphere of radius r_c that extends up to the radius where the outflow becomes optically thick:

$$r_c = r_{\rm ph,in}, \tag{5}$$

where $r_{\rm ph,\,in}$ is the inner photospheric radius of the outflow (see AZ). Following the observational evidence gathered from the X-ray spectral analysis (e.g. Pintore & Zampieri 2012; Pintore et al. 2014), we assume that the Compton parameter in the corona is significantly larger than unity and that Comptonization is saturated. In these assumptions, the high energy tail of the specific intensity of the source can be approximated with a Wien distribution (Rybicki & Lightman 1986):

$$I_\nu^W = \frac{2h\nu^3}{c^2} e^{-\alpha} e^{-h\nu/kT_c}, \tag{6}$$

where T_c is the electron temperature of the corona. Since Compton scattering conserves the photon number, the value of the factor $e^{-\alpha}$ is determined from the relation:

$$N_{\rm ph}^W = N_{\rm ph}^d. \tag{7}$$

Here, $N_{\rm ph}^d$ is the number of photons per unit time emitted from the disc which, for an observer at distance D, takes the form:

$$N_{\rm ph}^d = \pi \int_0^\infty \int_{r_{\rm in}}^{r_{\rm ph,in}} \left(\frac{I_\nu^d}{h\nu}\right) \frac{2r D^2}{(r^2+D^2)^2} {\rm d}r\,{\rm d}\nu, \tag{8}$$

while

$$N_{ph}^W = \pi \frac{r_c^2}{r_c^2 + D^2} \int_0^\infty \frac{I_\nu^W}{h\nu} {\rm d}\nu \tag{9}$$

is the number of photons which is emitted per unit time from the corona and r_{in} is the inner disc radius. In the following, we consider two reference electron temperatures for the corona: 1.2 and 1.5 keV. These temperatures sample the typical range of temperatures inferred from modelling the observed ULXs spectra (Pintore et al. 2014).

3.2 Model-data comparison

This section is dedicated to the comparison of our model with the optical and X-ray data of a few nearby ULXs. We constrain the model parameters using the photometric data and X-ray spectra of the sources. With the addition of an optically thick Comptonizing corona, our model can reproduce the multiwavelength emission of ULXs in an acceptable way, and can be effectively used to constrain the properties of ULXs. For each source analysed in this work, we proceed according to the following steps:

1. **Comparison with the CMD diagram**: The first step is to search the synthetic evolutionary tracks that intersect the optical emission of a ULX on the CMD. We search for intersections, when possible, in more than two colours, which provides an additional constraint.
2. **Age selection:** The comparison with the evolutionary tracks typically produces several intersections. Therefore, we select the model using an additional constraint, which is the age of the ULX inferred from the population study on the host environment.
3. **Search for the best fit of the multiwavelength SED:** Finally, after having selected the intersections matching the age of the ULXs, we computed the synthetic optical-through-X-ray SED of the correspondent snapshot of the track considering two electron temperatures of the optically thick corona: $kT_c = 1.2$ and 1.5 keV. The most representative SED is chosen applying a chi-square test to the data-model comparison. Although we remark that we are not adopting a data spectral fit, the chi-square test empowers the selection process. We applied our model to those ULXs that satisfy some specific criteria: (a) the compact object is unknown, (b) the optical counterpart has been univocally detected and analysed with *HST* data, (c) the ULXs have high X-ray luminosity. These sources are NGC 4559 X-7, NGC 5204 X-1, Holmberg II X-1 and NGC 5907 ULX-2. In addition, the age of the population to which NGC 4559 X-7 and Holmberg II X-1 belong is known, and we will use it as a further constraint to the model selection.

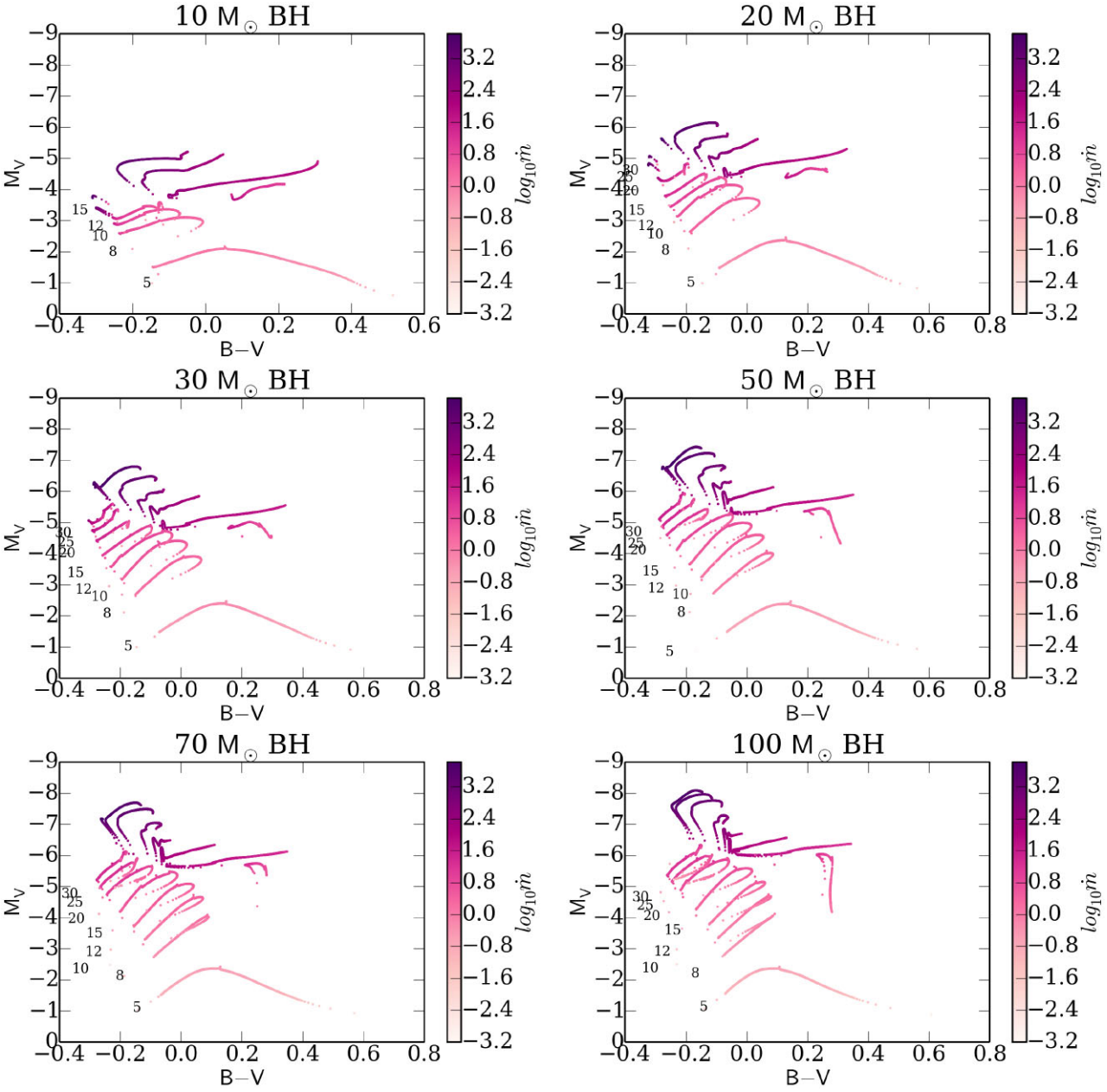

Figure 5. Evolutionary tracks on the CMD of the synthetic binary systems evolved with MESA: M_V versus $B - V$ colour.

3.2.1 NGC 4559 X-7

We follow Soria et al. (2005) and Tao et al. (2011) and assume a Galactic extinction $E(B - V) = 0.018$ and a distance of 10 Mpc [3] of the host galaxy. We consider the average of the magnitudes and colours taken from two measurements (Tao et al. 2011): F555W $= -7.05 \pm 0.08$ and F555W-F814W $= -0.11 \pm 0.13$. We take as reference age for this source the age of the parent population: ∼20 Myr (Soria et al. 2005). The position of the source on the CMD intersects the tracks of donors with initial mass of 15 $M_\odot$ accreting on to a 50 and 70 $M_\odot$ BH during the shell H-burning phase and tracks of evolved donors with initial mass of 12, 15, and 20 $M_\odot$ accreting on to a 100 $M_\odot$ BH. The age of all tracks of X-7 at intersection (∼15 Myr) are in agreement with that estimated from its stellar environment (∼20 Myr; Soria et al. 2005). We then fitted their multiwavelength SEDs to further constrain the models. We consider the *XMM–Newton* and *NuSTAR* observations of 2019 June (see Table 1). Indeed, the intersection of the ULX photometric point with a certain evolutionary track covers hundreds or thousands of years and fixes the average mass transfer rate at the Lagrangian point. The short-term fluctuations of the accretion rate and physical conditions in the system must be averaged out when performing this comparison. Therefore, the error bar of the X-ray spectrum encompasses the daily/monthly/yearly variability range of the source flux that is typically a factor of ∼2. Table 2 shows the best-fitting evolutionary tracks based on the χ^2 statistics: X-7 is reproduced with a system having donor of actual mass in the range of 5–6 $M_\odot$, accreting on to a massive BH with

[3]However, redshift-independent measurements suggest that the distance of NGC 4559 can be ∼7 Mpc [see Clark et al. (2018) and references therein]. We will discuss the implications of the distance estimation on our results later.

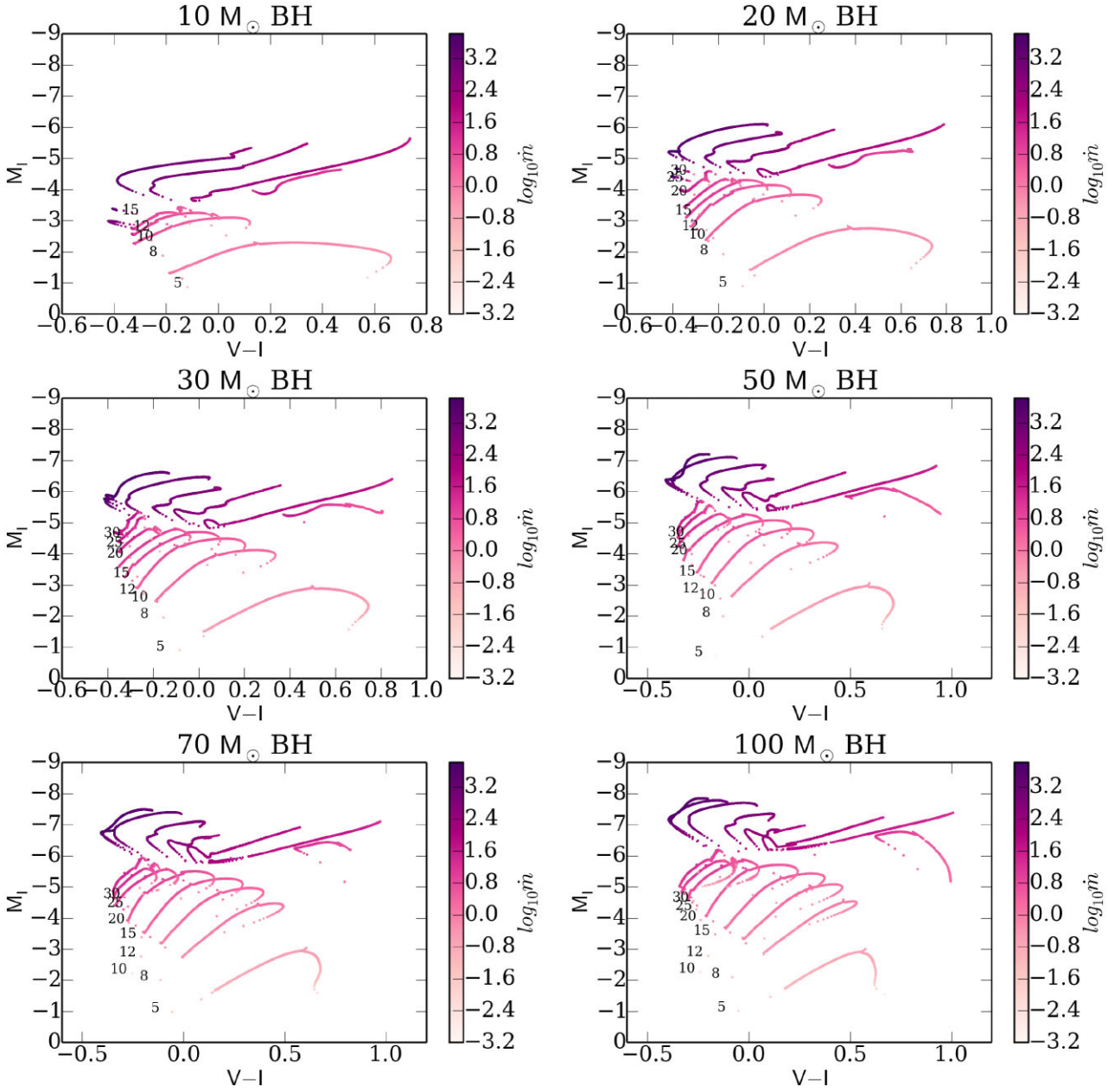

Figure 6. Evolutionary tracks on the CMD of the synthethic binary systems evolved with MESA: M_I versus $V - I$ colour.

Table 1. Log of the X-ray observations used in this work.

ULX	Instrument	Obs.ID	Date	Exp. (ks)
NGC 4559 X-7	*XMM–Newton*	0842340201	2019-06-16	74.3
	NuSTAR	30501004002	2019-06-17	94.9
NGC 5204 X-1	*XMM–Newton*	0693851401	2013-04-21	16.9
Hol II X-1	*XMM–Newton*	0200470101	2004-04-15	10.4
	NuSTAR	30001031002	2013-09-09	31.4
	NuSTAR	30001031003	2013-09-09	79.4
	NuSTAR	30001031005	2013-09-17	111
NGC 5907 X-2	*XMM–Newton*	0795712601	2017-12-01	60.8

actual mass of ∼56 $M_\odot$. Accretion on to a 70 and 100 $M_\odot$, BHs are excluded by the spectral fitting. The SED fit and the observed X-ray luminosity of X-7 (∼2 × 10^{40} erg s^{-1}; Soria et al. 2005) are better in agreement with a low corona temperature (Table 2). X-7 is well reproduced with a system accreting at largely super-critical rates on to a massive BH from donors that are ascending along the giant branch. Having lost most of their mass during the MS, are now less massive, with masses in the range of 5–6 $M_\odot$. The orbital period of this systems is quite long (>12 d, see Table 2) because the donor is evolved and has lost a large amount of mass. Fig. 7 shows that at these stages of the evolution, the optical emission is dominated by the outer accretion disc, which reaches a very high optical luminosity because of the high value of the mass transfer rate (dashed black line). At the same time, the very extended outflow dominates the UV/soft X-ray emission.

3.2.2 NGC 5204 X-1

NGC 5204 X-1 is located in the spiral galaxy NGC 5204 and has an average X-ray luminosity of 3 × 10^{39} erg s^{-1}. It is found to vary by

Table 2. Best-fitting models found minimizing the χ^2 for the sources analysed in this work.

NGC 4559 X-7								
Best fit model for systems with $M_{d,\,i} = 15$ M$_\odot$ and $M_{\rm BH,\,i} = 50$ M$_\odot$								
$k\,T_e$(keV)	t (Myr)	$M_d(t)$ (M$_\odot$)	$M_{\rm BH}$(t) (M$_\odot$)	$\dot{m}$	P (d)	$L_{\rm tot}$ (erg s^{-1})	χ^2	d.o.f.
1.2	15.3	5.5	55.8	$\sim 1 \times 10^3$	$\sim$18	3.2×10^{40}	72.2	40
NGC 5204 X-1								
Best-fitting model for systems with $M_{d,\,i} = 30$ M$_\odot$ and $M_{\rm BH,\,i} = 30$ M$_\odot$								
kT_e(keV)	t (Myr)	$M_d(t)$ (M$_\odot$)	$M_{\rm BH}(t)$ (M$_\odot$)	$\dot{m}$	P (d)	$L_{\rm tot}$ (erg s^{-1})	χ^2	d.o.f.
1.2	6.8	13.9	39	6.4	5.5	8.20×10^{39}	106.4	21
Holmberg II X1								
Best-fitting model for systems with $M_{d,\,i} = 20$ M$_\odot$ and $M_{\rm BH,\,i} = 50$ $M_\odot$								
kT_e(keV)	t (Myr)	$M_d(t)$ (M$_\odot$)	$M_{\rm BH}(t)$ (M$_\odot$)	$\dot{m}$	P (d)	$L_{\rm tot}$ (erg s^{-1})	χ^2	d.o.f.
1.2	$<$10	11.5	55	$\sim$10.5	5.5	1.3×10^{40}	31.7	36
NGC 5907 ULX-2								
Best-fitting model for systems with $M_{d,\,i} = 15$ M$_\odot$ and $M_{\rm BH,\,i} = 30$ M$_\odot$								
kT_e(keV)	t (Myr)	$M_d(t)$ (M$_\odot$)	$M_{\rm BH}(t)$ (M$_\odot$)	$\dot{m}$	P (d)	$L_{\rm tot}$ (erg s^{-1})	χ^2	d.o.f.
1.2	15.7	5.4	35.9	1890	$\sim$14	2.1×10^{40}	8.3	10

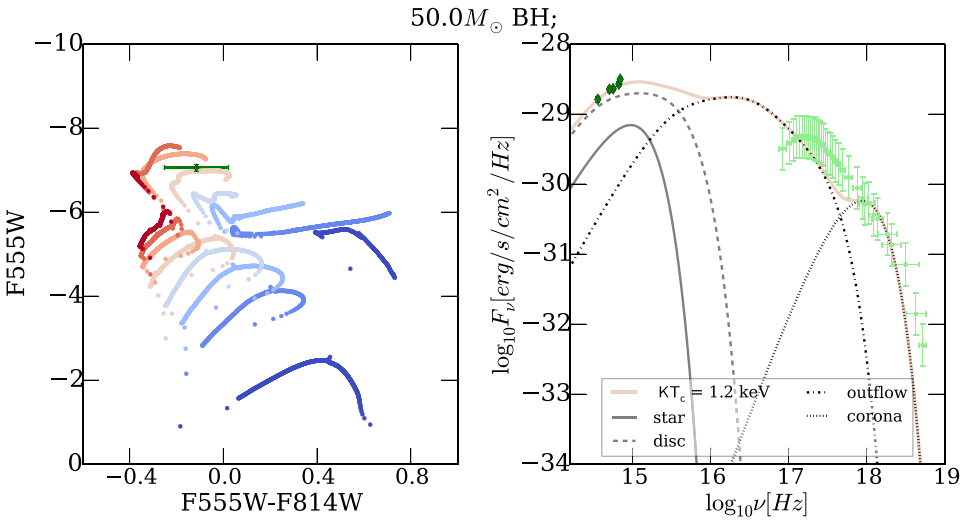

Figure 7. Left: Intersection of the optical counterpart of NGC 4559 X-7 (green point) with the evolutionary tracks of a 50 M$_\odot$ BH. Right: Total SED for the best-fitting solution together with the single spectral components. The total SED has the same colour of the evolutionary track (see left-hand panel) to which it belongs. Green and lightgreen points indicate optical and X-ray data, respectively.

$\sim$ 50 per cent in 10 yr (Liu, Bregman & Seitzer 2004). The source is thought to reside in a young stellar cluster with age $<$10 Myr (Goad et al. 2002). Among the data collected by Tao et al. (2011), we will consider the averages of those taken in August 2008: F555W $= -5.646 \pm 0.055$ and F450W $= -5.848 \pm 0.027$ adopting a distance of 4.3 Mpc and galactic extinction $E(B-V) = 0.013$. The optical counterpart of NGC 5204 X-1 is intersected by the tracks of donors with initial mass of 20 and 25 M$_\odot$ accreting on to a 20 M$_\odot$ BH at super-critical rates while the donor is ascending the giant branch; the track of a 20 M$_\odot$ donor accreting on to a 30 M$_\odot$ BH in the first stages of its H-shell burning phase, or the track of a donor with initial mass of 30 M$_\odot$ near the TAMS; the tracks of donors with initial mass 25 and 30 M$_\odot$ accreting on to BHs of 50, 70, and 100 M$_\odot$ during MS. These three cases differ in the evolutionary stages at which they occur: the more massive is the BH, the younger is the age of the system for the same initial donor mass, as we discussed in the previous section.

However, constraining the tracks with the age of the parent population does not help much, because the intersections are with tracks of very massive donors, whose evolution is very fast. We could rule out only the tracks of donors with initial mass of 25 M$_\odot$ that accrete on to BHs of 20 and 30 M$_\odot$. We then calculated the SED for all the other intersections and searched for the models that best fit our data, using only the X-ray spectrum of Liu et al. (2004) (see Table 1) and assuming an X-ray flux variability of 50 per cent.

Running through all the SEDs selected according to photometry and age, with the two aforementioned electron temperatures of the corona, leads us to exclude the majority of the models. The system which better reproduces the optical and X-ray data is the one with initial donor and BH mass of 30 M$_\odot$, with actual donor mass of about 13 M$_\odot$ and present BH mass of about 40 M$_\odot$ which undergoes marginal super-Eddington accretion during TAMS.

However, the fit is formally not statistically acceptable and the bolometric luminosity is not well reproduced. The reason for which the fit is not satisfactory is related to the fact that the last two points of the X-ray spectrum are not well reproduced (see Fig. 8).The source is harder than what predicted by our model and seems to require

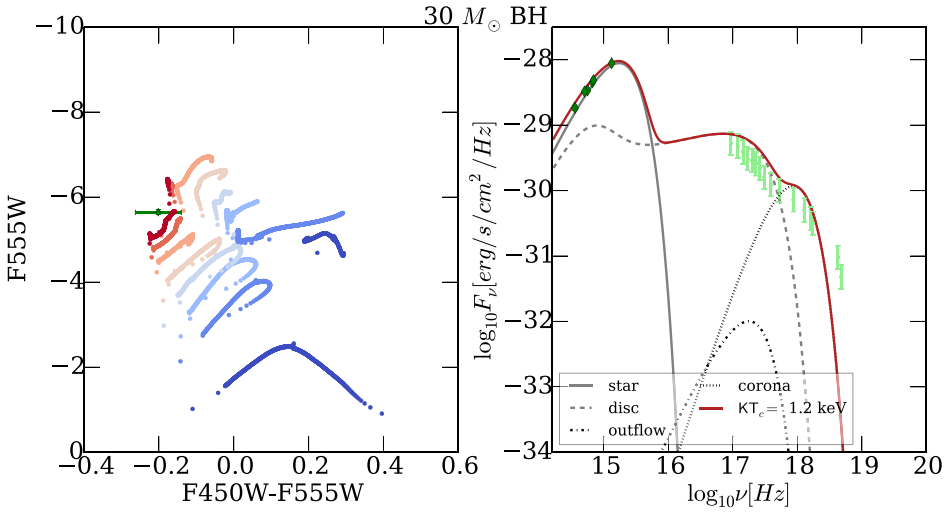

Figure 8. Left: Intersection of the optical counterpart of NGC 5204 X-1 (green point) with the evolutionary tracks of a 30M$_\odot$ BH. Right: Total SED for the best-fitting solution together with the single spectral components. The total SED has the same colour of the evolutionary track (see left-hand panel) to which it belongs. Green and lightgreen points indicate optical and X-ray data, respectively.

an additional component to fit the X-ray data points at the highest energies, as noted by Mukherjee et al. (2015).

3.2.3 *Holmberg II X-1*

Holmberg II X-1 is located in the dwarf irregular galaxy, Holmberg II, which is in the M81 group of galaxies at a distance of 3.05 Mpc (see Tao et al. 2011, 2012 and references therein). Its luminosity reaches $\sim 3 \times 10^{40}$ erg s^{-1} (Grisé et al. 2010). The source is surrounded by a photoionized optical nebula (Kaaret, Ward & Zezas 2004) containing a point-like optical counterpart. A study published by Egorov, Lozinskaya & Moiseev (2017) shows that X-1 is escaping from a very young cluster aged $\sim$ 3.5–4.5 Myr (Stewart et al. 2000), which will be the reference age for our study. We take the photometry from Tao et al. (2012) that reported the average fluxes of non-simultaneous observations in the F814W, F555W, F450W, and F336W filters: $(2.71 \pm 0.54) \times 10^{-18}$, $(7.74 \pm 1.55) \times 10^{-18}$, $(1.34 \pm 0.27) \times 10^{-17}$, and $(2.70 \pm 0.54) \times 10^{-17}$ erg s^{-1} cm^{-2}Å^{-1}, respectively. We search for intersections of the evolutionary tracks with data points on the CMD (calculated for different filters). Note that, because of the significant optical variability of the source, the error bar on the colour is large and the intersections of the data point with the simulated evolutionary tracks are numerous. Considering the very young age inferred by Stewart et al. (2000), the majority of the intersections are ruled out and we are left with systems accreting on to massive BHs (50 and 70 M$_\odot$) from donors with initial mass from 15 to 25 M$_\odot$. We then compared the SEDs obtained with our model with the observed optical through X-ray SED of Holmberg II X-1. The X-ray data are taken from Pintore et al. (2014) (see Table 1). Given the very young age, the majority of the best-fitting SEDs belong to systems in the sub-Eddington accretion phase, which can reproduce well the softer part of the X-ray spectrum but have a significantly different spectral energy distribution at the higher frequencies. The intersection that best fits the data is a system with an MS donor younger than 10 Myr with initial mass of 20 M$_\odot$ accreting on to a BH with initial mass of 50 M$_\odot$. The system is accreting marginally above Eddington ($\dot{m} \sim 10$). The actual mass of the donor is about 11 M$_\odot$ and that of the BH about 55 M$_\odot$. The orbital period is short ($P \sim 5.5$ d), because during the long and stable MS RLOF phase, the mass ratio of the system does not change dramatically (see Table 2). Fig. 9 shows that the SED that best fits the data is produced by a cool corona with an electron temperature of 1.2 keV. Moreover, being the accretion rate marginally super-critical, the outflow is not very extended and does not contribute much to the X-ray emission. Looking at the optical emission, it is dominated by the donor star but also the standard disc contributes in a significant way.

3.2.4 *NGC 5907 ULX2*

NGC 5907 ULX2 (Pintore et al. 2018) is located at a distance of 17.1 Mpc and it reached a peak X-ray luminosity of 6.4×10^{39} erg s^{-1}. Being a recent discovery, it is not well studied, and we do not have much information on its variability during the active phase. However, we know that the source is transient because in a previous observation taken in 2012, *Chandra* did not detect it (with an upper limit of 1.5×10^{38} erg s^{-1} on the X-ray luminosity). Clearly, our model does not take into account the disc instabilities that may lead to a transient behaviour. However, we can use it to approximately describe its active phase. We used the optical photometry and X-ray data presented in Pintore et al. (2018, see Table 1). Some of the synthetic tracks intersect with the photometric point of NGC 5907 ULX-2 on the CMD computed using the F450W magnitude and F450W-F814W colour. The source cannot be reproduced by systems accreting on to a 10 or 20 M$_\odot$ BH. On the basis of the photometry, the system can be a BH of 30 M$_\odot$ accreting from a donor which has an initial mass of 15 M$_\odot$, 50 M$_\odot$ from a donor with initial mass of 15 M$_\odot$, 70 M$_\odot$ from donors with initial mass of 12 and 20 M$_\odot$ and 100 M$_\odot$ from a donor with initial mass of 12 and 15 M$_\odot$.

For this source, we did not find information on the age of the host environment. Therefore, in the following, we considered all the snapshots that intersect the photometric point. Table 2 shows the result of the χ^2 test applied to the snapshots run for this source. The observed multiwavelength SED is better reproduced with a system composed of a donor star with mass of about 5.4 M$_\odot$ which is accreting at super-Eddington rates on to a BH of about 36 M$_\odot$. The system initially consisted of a 15 M$_\odot$ donor and a 30 M$_\odot$

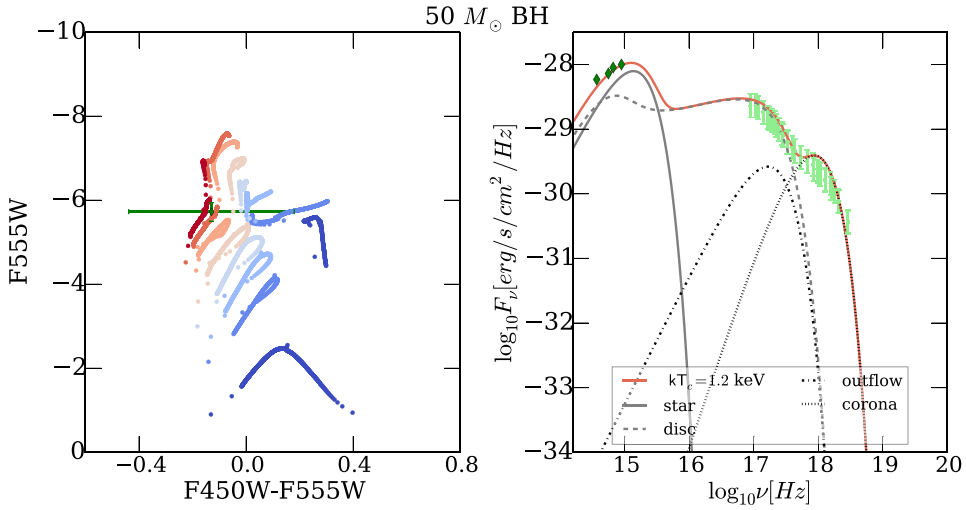

Figure 9. Left: Intersection of the optical counterpart of Holmberg II X-1 (green point) with the evolutionary tracks of a 50 $M_\odot$ BH. Right: Total SED for the best-fitting solution together with the single spectral components. The total SED has the same colour of the evolutionary track (see the left-hand panel) to which it belongs. Green and lightgreen points indicate optical and X-ray data, respectively.

BH. The accretion phase takes place while the donor is ascending along the Giant Branch. The binary has an orbital period of ~ 24 d, therefore the disc is very extended. In Fig. 10, we show the different components which contribute to the overall emission spectrum: the optical band is dominated by the outer accretion disc, which is very bright because of the very high mass transfer rate.

4 UNVEILING ULX PULSARS FROM OPTICAL DATA: AN EXPLORATORY STUDY

Since the discovery of the first pulsating ULX in 2014 (Bachetti et al. 2014), five other sources have been found to be accreting pulsars (Israel et al. 2017a, b; Carpano et al. 2018; Sathyaprakash et al. 2019; Rodríguez Castillo et al. 2019). Detecting pulsations likely requires a specific viewing angle and/or special physical conditions. If pulsars are not detected, it would be useful to have alternative approaches to distinguish between ULXs accreting on to a BH or an NS. In Pintore et al. (2017), a large sample of bright ULXs have been studied with the aim to search for specific signatures in the X-ray spectra that could be linked to the nature of the compact object. Above 2 keV, the spectra of the known ULX pulsars are harder than those of other ULXs analysed in their study. However, despite the effort, a clear spectral signature has not been found so far. Modelling the evolution and multiwavelength emission properties of ULX binary systems represents, in principle, an additional tool to assess the nature of the compact object and, at the same time, to understand the evolutionary paths that can lead to the formation of these systems (see PZ1, PZ2, and AZ). A detailed investigation of pulsars ULXs is beyond the scope of this paper. Here, we present only a preliminary study of the optical emission properties of ULX binary systems with a neutron star that undergo a transient (quasi-steady) RLOF accretion phase similar to that of massive donors in BH binaries. The purpose of the present investigation is simply to study the evolution of quite stable, low donor mass NS ULXs to get a grasp of their possible evolutionary paths and emission properties. High donor mass non-conservative systems are well beyond the present goals. Of course, the results presented here will not be relevant or applicable if all NS ULX binaries will definitely turn out to be system of the latter type.

4.1 Optical emission of pulsar ULXs

We used the evolutionary code MESA (Paxton et al. 2011, 2015) to evolve binaries with different masses accreting on to a neutron star. In this first exploratory study, we did not consider the magnetic field of the neutron star, because we are only interested in the optical emission that originates in the outer region. Moreover, we simplify the problem considering that the mass transfer is conservative, since non-conservative mass transfer on to NS from a massive donor is beyond the scope of this paper. Here, we show how the optical emission evolves under the following assumptions:

(i) A non-magnetized NS of 1.4 $M_\odot$;
(ii) Conservative mass transfer;
(iii) Case A mass transfer until the NS becomes very massive (we choose an upper limit of 2.5 $M_\odot$) or mass transfer becomes unstable;
(iv) Donor stars with masses in the range of 2–4 $M_\odot$.

This range of mass is broadly consistent with the donor of NGC 5907 ULX-1, which is thought to be an intermediate mass star in the range of 2–6 $M_\odot$ (Israel et al. 2017a); although the extinction in the direction of the source is very high (Heida et al. 2019). In addition, this assumption is also approximately consistent with the non-detection of the counterpart of M82 X-2, if its donor belongs to the lower end of the range obtained by Bachetti et al. (2014): $M_d \geq 5.2$ $M_\odot$.

More massive donors cannot steadily be evolved with this model. Given the low mass of the neutron star, we found that systems with donors more massive than 4 $M_\odot$ started abruptly dynamic unstable mass transfer. We show the evolution of two representative systems with an intermediate donor mass and a quite different q ratio.

4.1.1 Systems with donor of 2.5 $M_\odot$

When the RLOF phase of this system starts, accretion is super-Eddington, as it can be seen from the upper left panel of Fig. 11. The system initially shrinks (the upper right-hand panel of Fig. 11), then it starts to expand while the mass transfer decreases. After $\sim$4 Myr from the onset of RLOF, the neutron star mass reaches the critical value of 2.5 $M_\odot$ and the evolution is stopped.

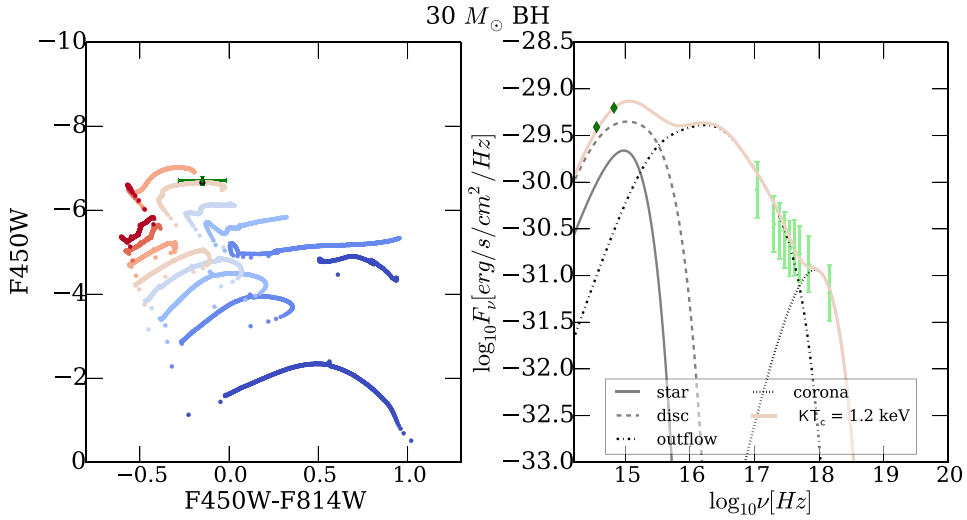

Figure 10. Left: Intersection of the optical counterpart of NGC 5907 X-2 (green point) with the evolutionary tracks of a 30 $M_\odot$ BH. Right: Total SED for the best-fitting solution together with the single spectral components. The total SED has the same colour of the evolutionary track (see left-hand panel) to which it belongs. Green and lightgreen points indicate optical and X-ray data, respectively.

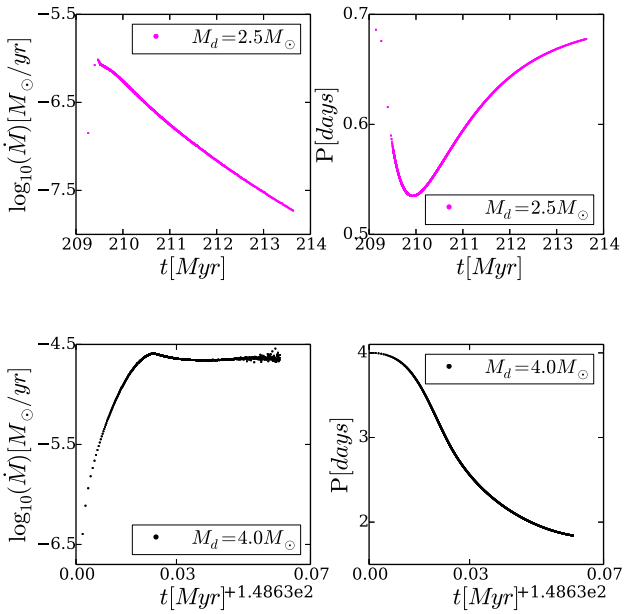

Figure 11. Upper panel: Evolution of the mass transfer rate (left) and the orbital period (right) for a system with a 2.5 $M_\odot$ donor and a 1.4 $M_\odot$ neutron star. Lower panel: The same for a system with a 4.0 $M_\odot$ donor. The mass transfer is supercritical at the onset of RLOF being the Eddington limit for a neutron star $\dot{M}_{\rm Edd,NS} \approx 10^{-8}\ M_\odot\ {\rm yr}^{-1}$.

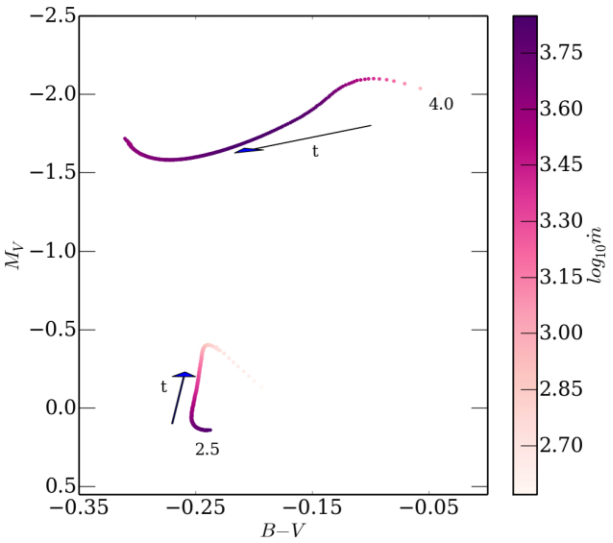

Figure 12. CMD in the $B-V$ colour and M_V magnitude for systems with donors of 2.5 (lower line) and 4 (upper line) $M_\odot$ accreting on to an NS with initial mass of 1.4 $M_\odot$. The colourmap represents the mass transfer rate normalized to the Eddington limit. The arrows indicate the direction of the evolution.

4.1.2 Systems with donors of 4 $M_\odot$

The system with a 4 $M_\odot$ donor starts accretion with a higher mass transfer rate than the previous case. During the short-lived RLOF phase ($\approx$7.0 $\times$ 10^4 yr), the system shrinks and the donor becomes unstable after having lost most of its mass.

4.1.3 Evolutionary tracks on the CMD

The evolutionary tracks on the CMD of the two binary pulsar ULXs described above are shown in Fig. 12, where the colourmap represents the magnitude of the mass transfer rate normalized to the Eddington limit of the evolving neutron star.

Both tracks have blue colours, but the *V*-band magnitude is very faint and considerably weaker than that of the evolutionary tracks of BH ULXs. The optical counterparts of ULX pulsars are essentially undetectable with *HST* if the masses of the donor stars are in the range of 2.5–4 $M_\odot$. This result is consistent with the non-detection of the counterpart of NGC 5907 ULX-1 (Sutton et al. 2013a; Heida et al. 2019). However, systems like NGC 7793 P13 that have a massive companion of 18–21 $M_\odot$ in an eccentric orbit (Israel et al. 2017b; Hu et al. 2017) cannot clearly be reproduced by a transient accretion phase of the type considered here.

5 SUMMARY AND CONCLUSIONS

We calculated an extended grid of evolutionary tracks of ULX binary systems with the MESA code. We considered a wide range of BH masses (10–100 $M_\odot$) and donor masses (5–30 $M_\odot$) and properly incorporated the orbital angular momentum loss in case of super-Eddington accretion with an outflow. For the calculation of the tracks, we adopted the model described in AZ. We found that they occupy two regions on the CMD, depending on the evolutionary stage of the donor.

When the donor is on the MS and accretion is sub-critical or marginally super-critical, the tracks are blue and their M_V magnitude is limited to ~ -6. They occupy the bluer and comparatively fainter corner of the CMD. We noticed that they are similar in shape for different BH masses, being the main difference the maximum value of M_V: more massive BHs generate more luminous tracks.

When the donor is ascending towards the Giant Branch, the properties of the evolutionary tracks are governed by the mass transfer rate, which is now super critical. Moreover, the binary separation increases rapidly producing a more extended accretion disc, which emits a huge amount of flux in the optical band, that can be enhanced by self-irradiation. This evolution drives the tracks towards higher *V*- band luminosities. The colours are initially blue because the mass transfer rate at the beginning of the Giant phase is very high and the disc is hot. As the super-Eddington mass transfer continues, the system widens and the accretion disc becomes more extended, driving the tracks towards redder colours. In addition, self-irradiation is essentially suppressed. However, after the peak, the mass transfer rate starts to decrease, irradiation starts to contribute again and for systems with more massive donors the evolution towards the red slows down.

In order to model the multiwavelength properties of ULXs we also included the contribution of saturated Comptonization from an inner spherical corona.

The data/model comparison proceeds through three sequential steps: comparison of the photometry with the evolutionary tracks on the CMD diagram, age selection, search for the best fit of the multiwavelength SED.

We applied our model to a number of ULXs with well-studied stellar optical counterparts: NGC 4559 X−7, NGC 5204 X−1, HolmbergII X−1, and NGC 5907 ULX−2.

(i) *NGC 4559 X-7:* The optical photometry of this source, together with the X-ray data, point to super-Eddington accretion on to massive BHs for this system. We found that the observed properties are reproduced by a system accreting above Eddington ($\dot{m} :\sim$ 900–1000) on to a BH of $\sim$55 $M_\odot$ from a donor of $\sim$5.5 $M_\odot$. The system consists of a standard disc emitting most of the optical luminosity, an optically thick and extended outflow which covers part of the standard disc and almost the entire inner advection dominated disc, and an optically thick cool corona, with electron temperature of $\sim$1.2 keV, which dominates the hard X-ray emission. The orbital period is fairly large, $\sim$18 d. In fact, when accretion occurs at super-critical rates, the orbital separation increases rapidly. The system produces very high bolometric luminosity [$(3 - 4) \times 10^{40}$ erg s^{-1}], which is in agreement with the observed data. The results obtained with the MESA tracks are in agreement with those obtained with the Eggleton evolutionary tracks (see AZ). This source was studied previously by other authors, and our results are in agreement with their findings. PZ found that the optical counterpart of X-7 is reproduced by a massive BH which accretes from a donor of 30–50 $M_\odot$ during the H-shell burning phase. Stobbart, Roberts & Wilms (2006) analysed some *XMM–Newton* observations of this source (which they refer to as NGC 4559 X-1) finding that its spectral shape is consistent with super-Eddington accretion on to BHs with masses up to 80 $M_\odot$.

However, the estimated value of the BH mass inferred from our model is strongly dependent on the assumed distance of the source, which affects the optical luminosity of the system and hence the match with the evolutionary tracks on the CMD. The distance of NGC 4559 is quite uncertain and estimates vary in the range of $\sim$6–15 Mpc. For a distance lower than the one assumed here (10 Mpc), like the redshift-independent distance adopted by Clark et al. (2018) ($d = 7.14$ Mpc), lower mass BHs, down to 20 $M_\odot$, would be inferred. In a recent work, Pintore et al. (2021) suggest the possibility that the compact object in NGC 4559 X-7 is even lighter, with a mass in the range of 1.4–4 $M_\odot$ (a light BH or a NS). A dedicated investigation of this scenario is outside the goals of this paper and we plan to do it in the future.

(ii) *NGC 5204 X-1:* The result obtained from the χ^2 fit of the SED at the time of intersection on the CMD suggests accretion at marginally super-critical rates from a donor with mass of $\sim$14 $M_\odot$ on to a BH with mass of $\sim$40 $M_\odot$. The system is 6.8 Myr old and accretion is taking place while the donor, whose initial mass is $\sim$30 $M_\odot$, is reaching the TAMS. However, the fit is not statistically acceptable and the bolometric luminosity is not well reproduced. The reason for which the fit is not satisfactory is related to the fact that the hard X-ray spectrum is not well represented. The source is harder than what predicted by our model and seems to require an additional high-energy tail to fit the X-ray data or a different geometry for comptonizing material. The existence of such a tail was studied by other authors. Mukherjee et al. (2015) modelled it with an additional Comptonizing component on the basis of the spectral analysis of coordinated *XMM* and *NuSTAR* observations of NGC 5204 X-1. A high energy excess with respect to a model with two thermal components has been found also by Walton et al. (2018), and was modelled with a cut-off power law component, produced by a possible accretion column, should the compact object being a NS.

(iii) *HolmbergII X-1:* The modelling of this source shows that this system is accreting at marginally super-Eddington rates. The BH may have a mass of about 55 $M_\odot$ while the donor star has $\sim$11 $M_\odot$. The best fit of the SED returns a corona temperature $\sim$1 keV. Kajava et al. (2012) studied the evolution of the spectral curvature of HolmbII finding that the accretion disc with advection (*diskpbb*[4] with $p \approx 0.5$ in XSPEC) fits the data better than the standard accretion disc (*diskbb*[5]). Moreover, adding a Comptonizing component reproduces the spectrum well if a low electron temperature is considered ($kT_e \approx$ 1.2 keV). Their findings are in agreement with the results obtained with our model.

(iv) *NGC 5907 ULX-2:* The observed multiwavelength SED is better reproduced with a system composed of a donor star with mass of about 4.5 $M_\odot$ which is accreting at super-Eddington rates on to a BH of about 36.5 $M_\odot$ according to the value suggested by Pintore et al. (2018) (where they adopted the model in AZ to infer a BH mass of 30 $M_\odot$). The system initially consisted of a 15 $M_\odot$ donor and a 30 $M_\odot$ BH. The accretion phase takes place while the donor is ascending along the Giant Branch. The binary has an orbital period of $\sim$24 d; therefore, the disc is very extended. As reported

[4]In the X-ray spectral fitting package XSPEC the *diskpbb* model is a multi-temperature blackbody disc model, where the local disc temperature T(r) is proportional to r^{-p}, where p is a free parameter (see Mineshige et al. 1994).
[5]In the X-ray spectral fitting package XSPEC the *diskbb* model refers to a multitemperature blackbody disc model, where the local disc temperature $T(r)$ is proportional to $r^{-3/4}$ (see Mitsuda et al. 1984).

by Pintore et al. (2018) the colour and luminosity of the optical counterpart are consistent with those of an O-B type star. From our modelling, it is clear that the contribution of the accretion disc to the optical emission is dominant. Therefore, the overall scenario can be misinterpreted if optical emission is ascribed only to the donor star. The outer standard disc contributes substantially to the optical flux mimicking the emission of a massive donor.

In summary, we found that two out of four ULXs are well represented by systems with BH mass in the range between 35 and 40 $M_\odot$, while for the other two the best-fitting solution points to more massive BHs, $\approx 55 M_\odot$. Therefore, although the present sample of ULXs is very small and not representative of the whole population, the observational emission properties, together with binary evolution and age estimates, seem to suggest the existence of massive BHs in some sources.

We finally explored the possibility to extend our model to the challenging case of PULXs. We could steadily evolve only systems with a maximum donor mass of 5 $M_\odot$, whose optical emission results to be too faint to be detected with *HST* at the observed distances of ULXs. This result is consistent with the non-detection of the counterpart of the Pulsar ULX NGC 5907 ULX-1 (Sutton et al. 2013a).

We note that two PULXs have a detected optical counterpart: NGC 7793 P13 and NGC 1313 X-2 (Grisé et al. 2008; Motch et al. 2014; Sathyaprakash et al. 2019). The first one is accreting from a massive donor (18–23 $M_\odot$; Israel et al. 2017b) and has been proved to be an eccentric binary system (Israel et al. 2017b; Hu et al. 2017). The optical counterpart of NGC 1313 X-2 is very luminous ($M_{V;\,B} < -4.5$) and cannot be reproduced with our evolutionary tracks for PULXs. Moreover, population studies reveal that its host environment is a young O-B association, aged $\approx$ 20 Myr, pointing to a young massive star for the donor. If compared with our model of accreting BHs, the optical counterpart of X-2 would be represented by a 25 $M_\odot$ BH that accretes at marginally super-Eddington rates from a 12 $M_\odot$ donor. The apparent degeneracy intrinsic to this result is broken by the value of the orbital period (see also AZ), which would be too long to be consistent with the range of periods proposed by Sathyaprakash et al. (2019).

Related to this, we emphasize the importance of a multiwavelength and multidisciplinary approach to unveil the nature of the binary systems that power ULXs. This would help to discern the nature of the accretor, whereas the possibility to detect coherent pulsation is halted by the poor quality of the data and/or the geometry of the system with respect to the observer or by the fact that pulsed emission is in fact not present. Despite the difficulties encountered by us and several authors in modelling accreting binaries with massive donors and a pulsars, these two sources show that accretion from a massive donor on to a neutron star is feasible. Possible scenarios could be different from that proposed in this work. Quast, Langer & Tauris (2019) show that nuclear timescale mass transfer is feasible for neutron star accretors with a different prescription for hydrogen and helium content of the donor star. El Mellah, Sundqvist & Keppens (2019) invoke accretion driven by Wind Roche lobe overflow. Another possibility is accretion under the hypothesis of eccentric orbits. All these scenarios need to be investigated in detail in the future in a framework similar to the one proposed here to assess the formation routes of NS-massive donors systems.

ACKNOWLEDGEMENTS

The authors thank the anonymous referee for their useful comments. EA acknowledges funding from the Italian Space Agency, contract ASI/INAF n. I/004/11/4. LZ also acknowledges financial support from the ASI/INAF grants 2017-14-H.0 and I/037/12/0, and from INAF grant 'Sostegno alla ricerca scientifica main stream' (INAF Presidential Decree 43/2018). AW also acknowledges financial support from the ASI/INAF grant no. 2017-14-H.0 and from INAF grant 'Sostegno alla ricerca scientifica main stream' (INAF Presidential Decree 43/2018). Simulations in this paper made use of the MESA code, the PYTHON language, and the packages MATPLOTLIB and MESA-reader. We also acknowledge the use of public data from the HEASARC archive and the XSPEC spectral fitting package.

DATA AVAILABILITY

All of the data underlying this article are already publicly available from ESA's *XMM–Newton* Science Archive (https://www.cosmos.esa.int/web/xmm-newton/xsa) and NASA's HEASARC archive (https://heasarc.gsfc.nasa.gov/).

REFERENCES

Ambrosi E., Zampieri L., 2018, MNRAS, 480, 4918 (AZ)
Bachetti M. et al., 2014, Nature, 514, 202
Belczynski K., Kalogera V., Rasio F. A., Taam R. E., Zezas A., Bulik T., Maccarone T. J., Ivanova N., 2008, ApJS, 174, 223
Belfiore A. et al., 2020, Nature Astron., 4, 147
Carpano S., Haberl F., Maitra C., Vasilopoulos G., 2018, MNRAS, 476, L45
Clark C. J. R. et al., 2018, A&A, 609, A37
Colbert E. J. M., Mushotzky R. F., 1999, ApJ, 519, 89
Copperwheat C., Cropper M., Soria R., Wu K., 2005, MNRAS, 362, 79
de Jager C., Nieuwenhuijzen H., van der Hucht K. A., 1988, A&AS, 72, 259
Ebisawa K., Życki P., Kubota A., Mizuno T., Watarai K.-Y., 2003, ApJ, 597, 780
Eggleton P., 2006, Evol. Proc. Bin. Multiple Stars, Available at: https://doi.org/10.1017/CBO9780511536205
Eggleton P., 2011, Evol. Proc. Bin. Multiple Stars, Available at: https://ui.adsabs.harvard.edu/abs/2011epbm.book.....E
Eggleton P. P., 1983, ApJ, 268, 368
Egorov O. V., Lozinskaya T. A., Moiseev A. V., 2017, MNRAS, 467, L1
El Mellah I., Sundqvist J. O., Keppens R., 2019, A&A, 622, L3
Fabbiano G., 1989, ARA&A, 27, 87
Fabrika S., Ueda Y., Vinokurov A., Sholukhova O., Shidatsu M., 2015, Nature Phys., 11, 551
Feng H., Kaaret P., 2008, ApJ, 675, 1067
Feng H., Soria R., 2011, New Astron. Rev., 55, 166
Gladstone J. C., Roberts T. P., Done C., 2009, MNRAS, 397, 1836
Glebbeek E., Gaburov E., de Mink S. E., Pols O. R., Portegies Zwart S. F., 2009, A&A, 497, 255
Goad M. R., Roberts T. P., Knigge C., Lira P., 2002, MNRAS, 335, L67
Grisé F., Pakull M. W., Soria R., Motch C., Smith I. A., Ryder S. D., Böttcher M., 2008, A&A, 486, 151
Grisé F., Kaaret P., Feng H., Kajava J. J. E., Farrell S. A., 2010, ApJ, 724, L148
Heida M., Harrison F. A., Brightman M., Fürst F., Stern D., Walton D. J., 2019, ApJ, 871, 231
Hu C.-P., Li K. L., Kong A. K. H., Ng C.-Y., Lin L. C.-C., 2017, ApJ, 835, L9
Israel G. L. et al., 2017a, Science, 355, 817
Israel G. L. et al., 2017b, MNRAS, 466, L48
Kaaret P., Ward M. J., Zezas A., 2004, MNRAS, 351, L83
Kaaret P., Feng H., Roberts T. P., 2017, ARA&A, 55, 303
Kajava J. J. E., Poutanen J., Farrell S. A., Grisé F., Kaaret P., 2012, MNRAS, 422, 990
Klencki J., Nelemans G., Istrate A. G., Pols O., 2020, A&A, 638, A55
Liu J.-F., Bregman J. N., Seitzer P., 2004, ApJ, 602, 249
Liu J.-F., Bregman J., Miller J., Kaaret P., 2007, ApJ, 661, 165
Makishima K. et al., 2000, ApJ, 535, 632

Mapelli M., Colpi M., Zampieri L., 2009, MNRAS, 395, L71
Mapelli M., Ripamonti E., Zampieri L., Colpi M., 2011, Astron. Nachr., 332, 414
Miller J. M., Fabian A. C., Miller M. C., 2005, preprint (astro-ph/0512552)
Mineo S., Gilfanov M., Sunyaev R., 2012, MNRAS, 419, 2095
Mineshige S., Hirano A., Kitamoto S., Yamada T. T., Fukue J., 1994, ApJ, 426, 308
Mitsuda K. et al., 1984, PASJ, 36, 741
Mizuno T., Kubota A., Makishima K., 2001, ApJ, 554, 1282
Motch C., Pakull M. W., Soria R., Grisé F., Pietrzyński G., 2014, Nature, 514, 198
Mukherjee E. S. et al., 2015, ApJ, 808, 64
Mushtukov A. A., Suleimanov V. F., Tsygankov S. S., Ingram A., 2017, MNRAS, 467, 1202
Pakull M. W., Mirioni L., 2002, preprint (astro-ph/0202488)
Pakull M. W., Grisé F., Motch C., 2006, in Meurs E. J. A., Fabbiano G., eds, IAU Symp. Vol. 230, Populations of High Energy Sources in Galaxies, Dublin, 15-19 Aug 2005. p. 293
Patruno A., Zampieri L., 2008, MNRAS, 386, 543 (PZ1)
Patruno A., Zampieri L., 2010, MNRAS, 403, L69 (PZ2)
Paxton B. et al., 2013, ApJS, 208, 4
Paxton B. et al., 2015, ApJS, 220, 15
Paxton B., Bildsten L., Dotter A., Herwig F., Lesaffre P., Timmes F., 2011, ApJS, 192, 3
Pinto C. et al., 2017, MNRAS, 468, 2865
Pinto C., Middleton M. J., Fabian A. C., 2016, Nature, 533, 64
Pintore F. et al., 2018, MNRAS, 477, L90
Pintore F. et al., 2021, MNRAS, 504, 551
Pintore F., Zampieri L., 2012, MNRAS, 420, 1107
Pintore F., Zampieri L., Wolter A., Belloni T., 2014, MNRAS, 439, 3461
Pintore F., Zampieri L., Stella L., Wolter A., Mereghetti S., Israel G. L., 2017, ApJ, 836, 113
Pols O., 2011, Bin. Stellar Evol., Lecture Notes
Poutanen J., Lipunova G., Fabrika S., Butkevich A. G., Abolmasov P., 2007, MNRAS, 377, 1187
Quast M., Langer N., Tauris T. M., 2019, A&A, 628, A19
Ramsey C. J., Williams R. M., Gruendl R. A., Chen C.-H. R., Chu Y.-H., Wang Q. D., 2006, ApJ, 641, 241
Renzo M., Ott C. D., Shore S. N., de Mink S. E., 2017, A&A, 603, A118
Roberts T. P., 2007, Ap&SS, 311, 203
Roberts T. P., Levan A. J., Goad M. R., 2008, MNRAS, 387, 73
Rodríguez Castillo G. A. et al., 2020, ApJ, 895, 60
Rybicki G. B., Lightman A. P., 1986, Radiative Processes in Astrophysics. Wiley-VCH, Germany
Sanbuichi K., Yamada T. T., Fukue J., 1993, PASJ, 45, 443
Sathyaprakash R. et al., 2019, MNRAS, 488, L35
Smith N., 2014, ARA&A, 52, 487
Soberman G. E., Phinney E. S., van den Heuvel E. P. J., 1997, A&A, 327, 620
Soria R., Cropper M., Pakull M., Mushotzky R., Wu K., 2005, MNRAS, 356, 12
Stewart S. G. et al., 2000, ApJ, 529, 201
Stobbart A.-M., Roberts T. P., Wilms J., 2006, MNRAS, 368, 397
Sutton A. D., Roberts T. P., Gladstone J. C., Farrell S. A., Reilly E., Goad M. R., Gehrels N., 2013a, MNRAS, 434, 1702
Sutton A. D., Roberts T. P., Middleton M. J., 2013b, MNRAS, 435, 1758
Tao L., Feng H., Grisé F., Kaaret P., 2011, ApJ, 737, 81
Tao L., Kaaret P., Feng H., Grisé F., 2012, ApJ, 750, 110
van den Heuvel E. P. J., 1994, in Shore S. N., Livio M., van den Heuvel E. P. J., Nussbaumer H., Orr A., eds, Saas-Fee Advanced Course 22: Interacting Binaries. p. 263
Vink J. S., de Koter A., Lamers H. J. G. L. M., 2000, A&A, 362, 295
Vink J. S., de Koter A., Lamers H. J. G. L. M., 2001, A&A, 369, 574
Walton D. J. et al., 2018, MNRAS, 473, 4360
Wolter A., Esposito P., Mapelli M., Pizzolato F., Ripamonti E., 2015, MNRAS, 448, 781
Wolter A., Fruscione A., Mapelli M., 2018, ApJ, 863, 43
Zampieri L., Roberts T. P., 2009, MNRAS, 400, 677

APPENDIX A: $Z = 0.2\ Z_{\odot}$, BH = 20 $M_{\odot}$

Effects of metallicity on the binary evolution of systems that undergo case A mass transfer. We show the representative case of accretion on to a BH of 20 $M_{\odot}$ for donors with solar and sub-solar ($Z = 0.2\ Z_{\odot}$) metallicity. Metallicity does not induce important changes on the evolution of donors for case A mass transfer. Fig. A1 shows the evolution of the mass transfer rate for systems with donor with 8, 10, 20, 25 and 30 $M_{\odot}$. The mass transfer rate evolves similarly in the two cases, with a slight delay in time and shortening in the duration of the main accretion episode.

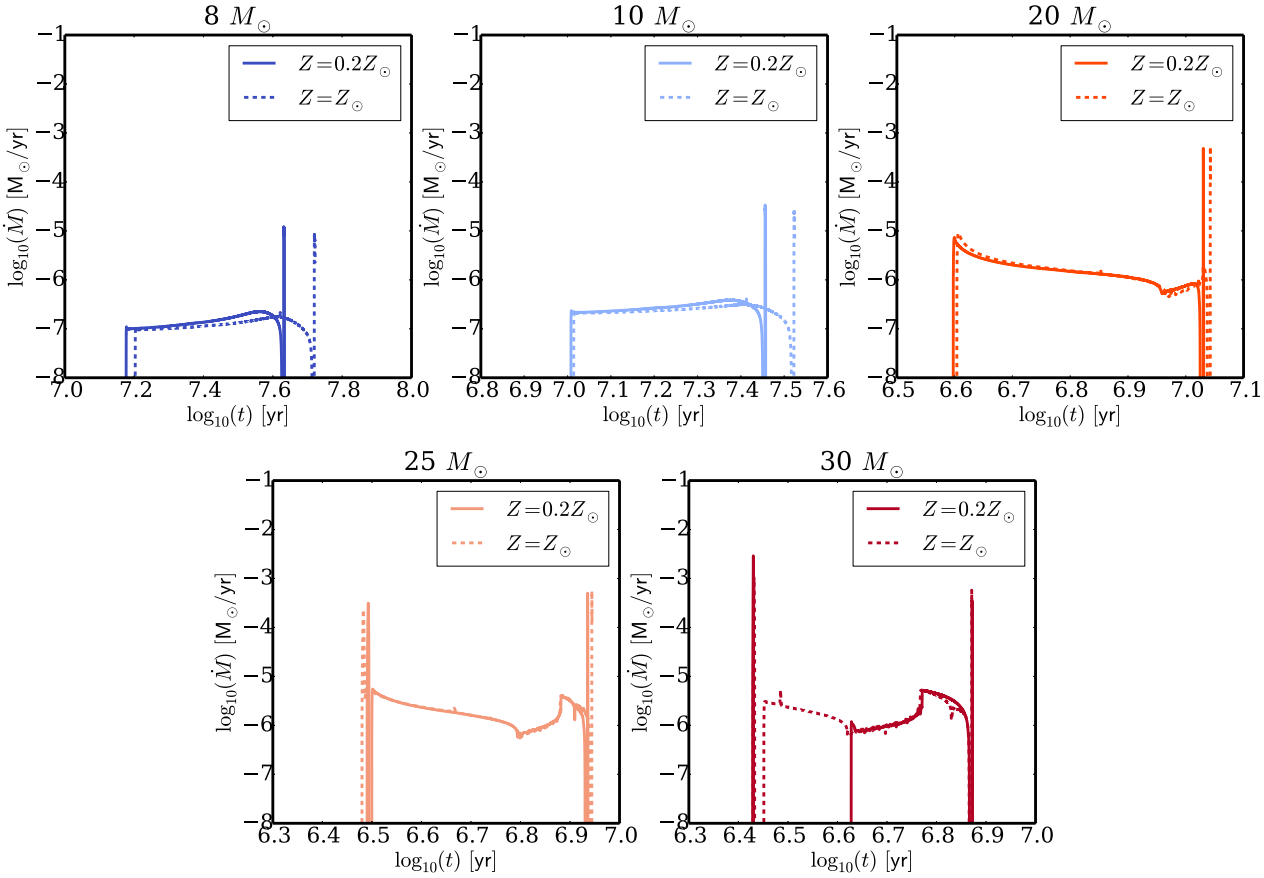

Figure A1. Evolutionary tracks for systems with same donor mass and BH mass, but different metallicities.

APPENDIX B: EVOLUTIONARY TRACKS FOR A GIVEN BH MASS

B1. Systems accreting onto a 10 $M_\odot$ *BH*

The evolutionary tracks on the CMD for systems accreting on to a 10 $M_\odot$ BH are shown in the upper left-hand panel of Figs 5 and 6. We notice first that the track of the 20 $M_\odot$ donor does not appear in the CMD, while that of a 15 $M_\odot$ donor is only marginally represented. During the first contact episode during MS, these systems accrete at very high super-Eddington rates (see the upper left-hand panel of Fig. 1) so that the outflow engulfs the binary and we cannot follow their evolution with our model. We are left with the systems accreting from less massive donors: from 5 to 12 $M_\odot$.

When the donors are on the MS, the tracks are blue ($B-V \simeq -0.3$: 0.0) and not very luminous ($M_V \simeq -2$: -3.5). The 5 $M_\odot$ donor represents an exception (see below): during MS it becomes redder ($B-V$ increases up to 0.5) and its luminosity progressively decreases ($M_V \simeq -1$: -2.3).

When the donors evolve off the MS and the mass transfer becomes super-Eddington, colours are initially blue and then they become redder. The magnitudes are brighter than in MS, in the range $M_V = -3.8$: -5.2.

As mentioned above, the 5 $M_\odot$ donor behaves in a different way. First, the radius of the disc at the TAMS is larger than that of the other systems. Moreover, the mass transfer rate is considerably sub-Eddington. These two facts imply that the accretion disc is relatively cold. Also the donor star, which at TAMS is a low-mass star (see Fig. 3), is relatively weak and cold. Therefore, the V magnitude of the system is weak and colours are red ($B-V \sim 0.5$). Given the low star and disc temperatures, the system with a 5 $M_\odot$ donor is more luminous in the I band than in the V band, as it can be seen comparing Fig. 5 with Fig. 6.

B2. Systems accreting onto a 20 $M_\odot$ *BH*

Let now consider the CMDs for systems accreting on to a 20 $M_\odot$ BH (upper right panel of Figs 5 and 6). At variance with the previous case, the tracks belonging to all the donor stars appear in the diagram. In fact, the lower value of the mass ratios (Fig. 3) allows for a less eruptive initial mass transfer phase. We could evolve steadily the 15 $M_\odot$ donor. The track of a 20 $M_\odot$ donor is stopped only at the final stages of the giant branch. More massive donors (25 and 30 $M_\odot$) are evolved for a short time and then their evolution is stopped because the outflow engulfs the binary.

The evolution of the optical properties of these systems are similar to those described above for a 10 $M_\odot$ BH. The only difference is that $V-I$ colours are redder than the those of systems with a 10 $M_\odot$ BH, because the discs are more extended. The evolution of the 5 $M_\odot$ donor during MS is different, because the system is accreting sub-Eddington (as for the 10 $M_\odot$ BH).

For the more massive donors ($M > 10M_\odot$), the accretion in the post MS phases is characterized by blue colours and bright M_V magnitude ($B-V \sim -0.23$: 0.0, $M_V \sim -5.0$: -6.3). For lower mass donors ($M \leq 10M_\odot$), systems are comparatively redder and fainter ($B-V \simeq 0$: 0.6, $V-I \sim -0.2$: 0.8, $M_V \sim -4.0$: -5.3, $M_I \sim -4.5$: -6.1).

B3. Systems accreting onto a 30 $M_\odot$ *BH*

For a 30 $M_\odot$ BH accretion is more stable from the beginning of the RLOF for donors up to 30 $M_\odot$ (middle left-hand panel of Fig. 1). For a given mass the binary separation is larger. This prevents the outflow from engulfing the binary during MS. All the systems with donor mass $M_d \leq 25$ $M_\odot$ can be evolved with our model, while the system with donor mass $M_d = 30$ $M_\odot$ is stopped at the middle of the giant phase. For donors less massive than 20 $M_\odot$ during MS, the flux emitted by the disc overcomes that emitted by the star (see Appendix C). The evolution of the optical emission is essentially similar to that of the 10 and 20 $M_\odot$ BH case.

When systems exit the MS the flux of the disc is dominant and the emission is super-Eddington. The tracks of more massive donors remain blue, and luminous ($B - V \sim -0.0$: -0.05, $V - I \sim -0.4$: 0.1, $M_V = -5.1$: -6.9, $M_I \sim -5.0$: -6.7). Systems with less massive donors turn into redder colours and are slightly less luminous ($B - V \sim -0.1$: 0.4, $V - I \sim -0.3$: 0.9, $M_V = -1.5$: -5.5, $M_I \sim -4.5$: -6.5).

B4. Systems accreting onto a 50 $M_\odot$ *BH*

For a 50 $M_\odot$ BH (the middle right-hand panel of Figs 5 and 6) only the track with the donor of 30 $M_\odot$ is truncated when the outflow engulfs the binary. The post-MS phases, characterized also in this case by super-Eddington accretion, follow the trend described above. The range of colors and magnitudes of these systems during the super-Eddington accretion phases are: $B - V \sim -0.1$: 0.4, $V - I \sim -0.4$: 1.0, $M_V = -5.2$: -7.5, $M_I \sim -5.4$: -7.2

B5. Systems accreting onto a 70 $M_\odot$ *BH*

For a 70 $M_\odot$ BH (lower left panel of Figs 5 and 6), the evolution of the systems is similar to that of the 50 $M_\odot$ BH. Also in this case, the track of the 30 $M_\odot$ donor is interrupted because the outflow becomes too extended. The tracks are similar to the 50 $M_\odot$ case but slightly redder, being the accretion disc larger. Magnitude and colours during MS are in the range: $B - V \sim -0.3$: 0.6, $V - I \sim -0.4$: 0.5, $M_V = -2.5$: -6.0, $M_I \sim -2.8$: -5.9, while during the post-MS phases are in the range: $B - V \sim -0.1$: 0.4, $V - I \sim -0.4$: 1.0, $M_V = -5.5$: -7.8, $M_I \sim -5.8$: -7.7.

B6. Systems accreting onto a 100 $M_\odot$ *BH*

Finally, we describe the evolution of systems accreting on to a 100 $M_\odot$ BH, which is the maximum BH mass considered in this work (lower right panels in Figs 5 and 6). Even for the high mass transfer rate which characterizes the initial evolution of a 30 $M_\odot$ donor (see Fig. 1), the outflow does not engulf the system. We can evolve it up to the moment in which the donor starts He-burning in the nucleus, which is the endpoint of the evolutionary tracks we evolved with MESA.

The behaviour is similar to that of the systems with a 50 or 70 $M_\odot$ BH. The systems become very red and the luminosity in the V band increases significantly. Magnitude and colours, during MS are in the range: $B - V \sim -0.3$: -0.1, $V - I \sim -0.45$: 0.5, $M_V = -2.5$: -6.3, $M_I \sim -2.3$: -6.1, while during the post-MS phases are in the range: $B - V \sim -0.25$: -0.1, $V - I \sim -0.4$: 0.1, $M_V = -6.0$: -8.2, $M_I \sim -6.1$: -7.9.

APPENDIX C: FLUX RATIOS

In this appendix, we show the ratios between the flux emitted by the disc and that emitted by the star in the V band (Fig. C1). These figures help to understand the evolutionary tracks on the CMD described in Section 2.2.

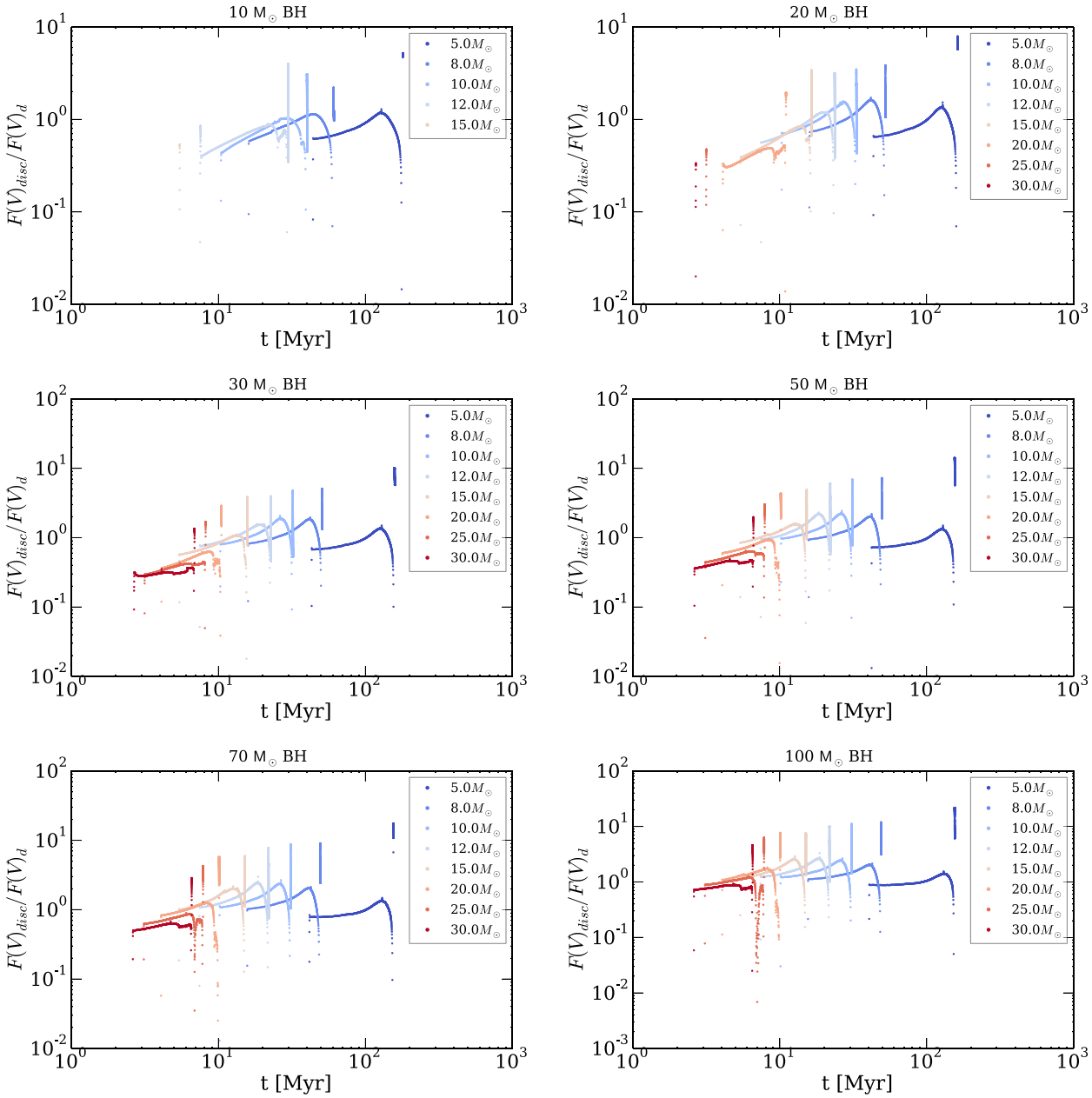

Figure C1. Evolution of the ratio between the flux emitted by the disc and that emitted by the donor star in the Johnson *V* filter. The trend of the tracks while the donor is on the MS is considerably influenced by the flux ratio.

This paper has been typeset from a TEX/LATEX file prepared by the author.